ISSN 0869-5911, Petrology, 2007, Vol. 15, No. 5, pp. 488–508. © Pleiades Publishing, Ltd., 2007.
Original Russian Text © A.B. Perepelov, M.Yu. Puzankov, A.V. Ivanov, T.M. Filosofova, E.I. Demonterova, E.V. Smirnova, L.A. Chuvashova, T.A. Yasnygina, 2007, published in Petrologiya, 2007, Vol. 15, No. 5, pp. 524–546.

Neogene Basanites in Western Kamchatka: Mineralogy, Geochemistry, and Geodynamic Setting

A. B. Perepelov[a], M. Yu. Puzankov[b], A. V. Ivanov[c], T. M. Filosofova[b], E. I. Demonterova[c], E. V. Smirnova[a], L. A. Chuvashova[a], and T. A. Yasnygina[c]

[a] *Vinogradov Institute of Geochemistry, Siberian Division, Russian Academy of Sciences, ul. Favorskogo 1a, Irkutsk, 664033 Russia*
e-mail: region@igc.irk.ru

[b] *Institute of Volcanology and Seismology, Far East Division, Russian Academy of Sciences, bul'v. Piipa 9, Petropavlosk-Kamchatskii, 683006 Russia*
e-mail: puzankov@kscnet.ru

[c] *Institute of the Earth's Crust, Siberian Division, Russian Academy of Sciences, ul. Lermontova 128, Irkutsk, 664033 Russia*
e-mail: aivanov@crust.irk.ru

Received July 13, 2005

Abstract—Neogene (N_1^2–N_2^1?) K–Na alkaline rocks were found in western Kamchatka as a subvolcanic basanite body at Mount Khukhch. The basanites have a microphyric texture with olivine phenocrysts in a fine-grained doleritic groundmass. The olivine contains inclusions of Al–Cr spinel. The microlites consist of clinopyroxene, plagioclase, magnetite, and apatite, and the interstitial phases are leucite, nepheline, and analcime. The Mount Khukhch basanites are characterized by elevated concentrations of MgO, TiO_2, Na_2O, and K_2O, high concentrations of Co, Ni, Cr, Nb, Ta, Th, U, LREE (La_N/Yb_N = 10.8–12.6, Dy_N/Yb_N = 1.4–1.6) at moderate concentrations of Zr, Hf, Rb, Ba, Sr, Pb, and Cu. The values of indicator trace-element ratios suggest that basanites in western Kamchatka affiliate with the group of basaltoids of the within-plate geochemical type: Ba/Nb = 10–12, Sr/Nb = 17–18, Ta/Yb = 1.3–1.6. The basanites of western Kamchatka show many compositional similarities with the Miocene basanites of eastern Kamchatka, basanites of some continental rifts, and basalts of oceanic islands (OIB). The geochemistry of these rocks suggests that the basanite magma was derived via the ~6% partial melting of garnet-bearing peridotite source material. The crystallization temperatures of the first liquidus phases (olivine and spinel) in the parental basanite melt (1372–1369°C) and pressures determined for the conditions of the "mantle" equilibrium of the melt (25–26 kbar) are consistent with the model for the derivation of basanite magma at the garnet depth facies in the mantle. The geodynamic environment in which Neogene alkaline basaltic magmas occur in western Kamchatka was controlled by the termination of the Oligocene–Early Miocene subduction of the Kula oceanic plate beneath the continental margin of Kamchatka and the development of rifting processes in its rear zone. The deep faulting of the lithosphere and decompression-induced magma generation simultaneous with mantle heating at that time could be favorable for the derivation of mantle basite magmas.

DOI: 10.1134/S0869591107050049

INTRODUCTION

Newly obtained data on the evolution of within-plate magmatism near the convergent boundaries of lithospheric plates attract much attention of geologists and petrologists, because they impose fairly severe constraints onto model proposed for the magmatic and geodynamic evolution of these environments. The identification of spatiotemporal relations between within-plate and subduction-related arc magmatism in active continental margins is important for petrogenetic models and for testing certain issues of various geodynamic concepts.

Recent studies in the Kamchatka arc system have resulted in the discovery of K–Na subalkaline and alkaline basaltoid rock complexes of various ages belonging to the within-plate geochemical type. These finds were expectable, because the tectonic and magmatic evolution of the structure of Kamchatka throughout the whole Cenozoic was controlled by the multiple changes in the geodynamic regimes and accompanied processes not only of subduction and accretion–collision of lithospheric plate but also of rifting (Legler, 1977; Solov'ev et al., 1998; Bogdanov and Chekhovich, 2002, 2004; Konstantinovskaya, 2003).

Subalkaline and alkaline basaltoids of the within-plate geochemical type were found in Miocene volcanic–sedimentary sequences in eastern Kamchatka (Volynets et al., 1990a, 1997), where they are thought to have been related to the termination of the Oligocene–Miocene subduction of the Kula oceanic plate

beneath the continental margin of Kamchatka as a result of the accretion of the Kronotskii island arc. The volcanic complexes of the Sredinnyi Range in Kamchatka include a Late Pliocene–Early Quaternary alkaline basalt–trachyte–comendite and Late Pleistocene–Holocene alkaline olivine basaltic rock series in close spatiotemporal association with typical arc volcanic series (Volynets, 1993, 1994; Churikova et al., 2001; Ivanov et al., 2004). Similar alkaline olivine basalts were found among the lavas of Quaternary Nachikinskii volcano north of the Aleutians–Kamchatka junction of arc structures (Portnyagin et al., 2005) and near Bakening volcano (Dorendorf et al., 2000). Basaltoids of the K–Na subalkaline and alkaline series of the Sredinnyi Range show compositional characteristics intermediate between those of magmatic rocks of the within-plate and island-arc geochemical types, and the genesis of these rocks remains disputable. Some researchers believe that the lithosphere beneath Kamchatka includes a source of OIB magmas (a source of oceanic island basalts), which participates in the generation of alkaline basaltic magmas and produces melts of the arc geochemical type (Churikova et al., 2001). Other authors address to some particular conditions under which magmas are derived in subduction zones (Tatsumi et al., 1995).

In the rear zone of the Kamchatka arc system, the large Western Kamchatka tectono–stratigraphic zone was determined to contain widespread alkaline and subalkaline basaltoid complexes of Paleogene–Neogene age (absarokites, trachybasalts, and shonkinites) (Volynets et al., 1987, 1990b; Volynets, 1993). In contrast to the K–Na subalkaline and alkaline rock series of the within-plate geochemical type, the latter are characterized by clearly pronounced enrichment in K_2O and by low and moderate HFSE concentrations. The geochemistry of the potassic alkaline and subalkaline basaltoids in western Kamchatka imply that their parental magmas were derived from sources containing the material of extensively metasomatized phlogopite-bearing rocks of the upper mantle, and the genesis of these rocks is thought to have been related to magma generation in a postsubduction geodynamic environment (Volynets et al., 1987; Perepelov et al., 2001, 2003).

In spite of numerous geologic–tectonic reconstructions suggesting that the Cenozoic was marked by widespread rifting (see, for example, Bogdanov and Chekhovich, 2004), magmatic rocks of the within-plate geochemical type have never before been found in western Kamchatka. Nevertheless, the age and structural setting of alkaline and subalkaline magmatism in western Kamchatka, where these processes were restricted to periods of time when active subduction terminated, do not rule out the occurrence of typical within-plate magmatic rocks in this territory.

During the 2001 fieldwork under a program on studying potassic alkaline magmatism in western Kamchatka, a Neogene subvolcanic body of basanites was found in the basin of the Bystraya River. The mineralogical and geochemical data obtained on these basanites and some geodynamic conclusions are discussed in this paper.

PREEXISTING DATA AND THE GEOLOGICAL SETTING OF THE BASANITES

Information on K–Na subalkaline and alkaline magmatic rocks in western Kamchatka is scarce, and the geochemical characteristics of these rocks are either absent or do not confirm their affiliation with the within-plate geochemical type. For example, magmatic complexes in western Kamchatka were found out to include Late Paleogene subvolcanic bodies of K–Na shonkinites and syenites, but these rocks differ from typical within-plate magmatic rocks by certain geochemical features, such as moderate HFSE concentrations, and high concentrations of K, Ba, and Sr (Perepelov et al., 2001, 2003). Moreover, an Early Quaternary stock of leucite basanites was discovered and studied in the course of geological survey and specialized geological operations in the basin of the Khlebnaya River (Moroz, 1971) (Fig. 1). According to Guziev (1967), Pliocene magmatic rocks of similar composition were also found near Utkholok Cape, but these rocks were classed with limburgite basaltoids. In 1982, data obtained on the stock at the Khlebnaya River have demonstrated that the rocks should be attributed to the group of analcime trachybasalts with elevated concentrations of Ba, Zr, and F and low Ti concentrations. Neither leucite nor pseudoleucite were found in these rocks (Volynets et al., 1986, sample KT-627). When geophysical data on the sedimentary sequences in western Kamchatka and adjacent part of the Sea of Okhotsk were interpreted, some researchers pointed to the pres-

Fig. 1. Schematic map for volcanic belts in Kamchatka showing the localization of the Mount Khukhch basanites (modified after *Geological Map*…, 2005).

(1) Paleogene sedimentary sequences with Eocene–Early Oligocene subvolcanic bodies of rocks of potassic alkaline and subalkaline series in western Kamchatka (absarokites, trachybasalts, shonkinites, and syenites); (2) Paleocene–Middle Eocene volcanic belt in western Kamchatka (Shantser and Fedorov, 1999); (3) Miocene sedimentary sequences with Middle–Late Miocene subvolcanic bodies and lavas of K–Na alkaline and subalkaline basaltoids in eastern Kamchatka; (4) Oligocene–Miocene and Pliocene–Quaternary volcanic belts in Southern Kamchatka (*SK*), eastern Kamchatka (*EK*), and the Sredinnyi Range (*SR*); (5) subvolcanic basanite body at Mount Khukhch (triangulation height 306.5 m), western Kamchatka, coordinates: 56° 25' N, 157° 26' E; (6) sampling sites of unconfirmed basanites and limburgite basalts in western Kamchatka (stocks: KH—Mount Khlebnaya, U—Utkholok Cape), E—stock at Mount Emguchan' (hypothetical analogues of the Mount Khukhch basanites). CKD—Central Kamchatka Depression.

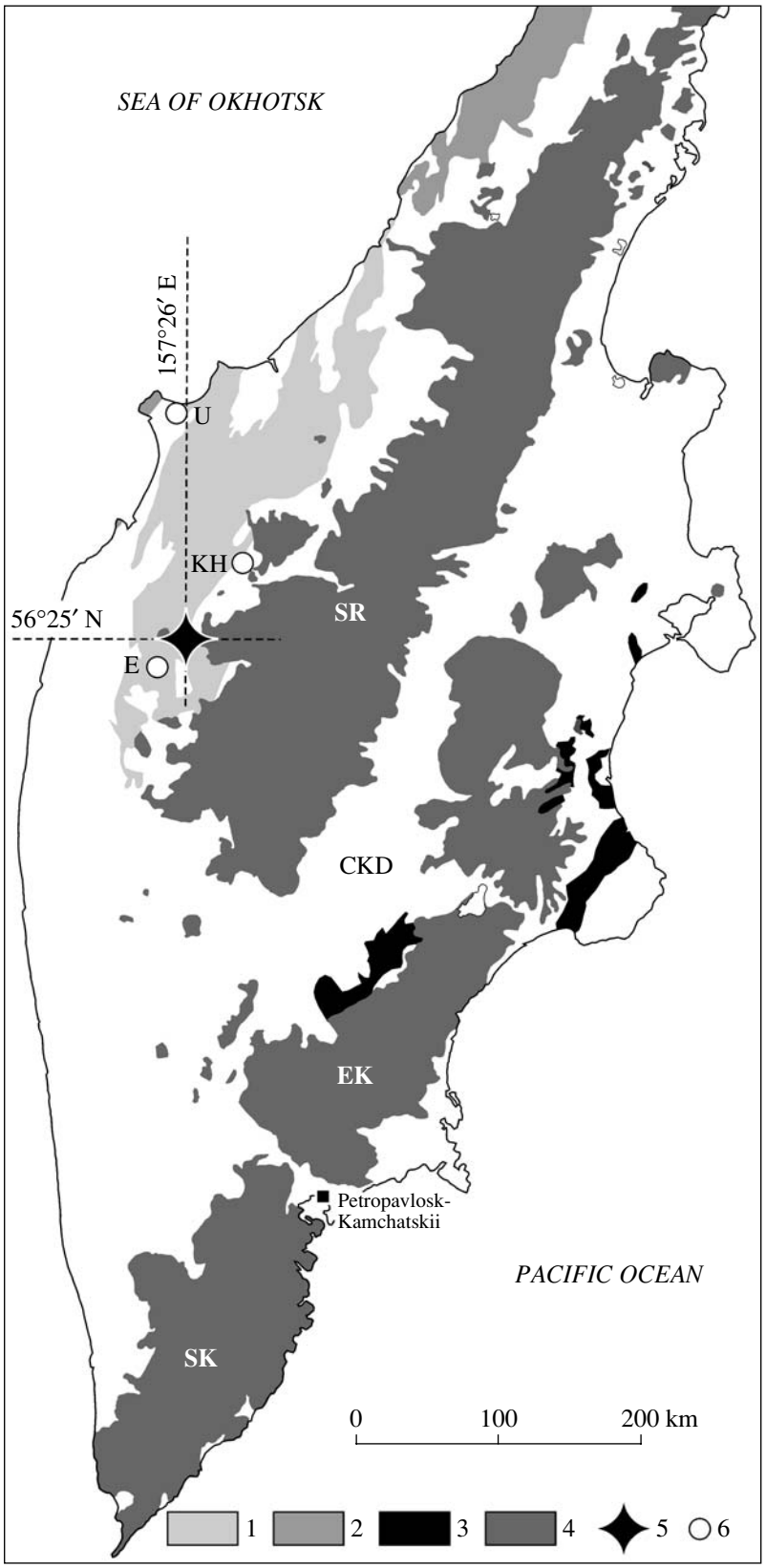
SEA OF OKHOTSK
157°26′ E
U
KH
56°25′ N
SR
E
CKD
EK
Petropavlosk-
Kamchatskii
PACIFIC OCEAN
SK
0
100
200 km
1
2
3
4
5
6

ence of a series of magmatic bodies at deep levels of the structure, with these bodies related to rifting processes. However, no exposures of these rocks were found at the surface (Antipov et al., 1997).

In the middle reaches of the Bystraya and Belogolovaya rivers, subvolcanic bodies of trachybasalts were studied at mounts Khukhch and Emguchan' (Fig. 1) in the course of geological survey (Koval' and Adamchuk, 1986). The composition and petrography of these rocks turned out to be closely similar. Three subvolcanic bodies discovered near the summit of Mount Khukhch were interpreted as variably oriented trachybasalt dikes, and the body at Mount Emguchan' was interpreted as a trachybasalt stock. Judging by the reported bulk compositions, these rocks are high-Mg K–Na subalkaline basaltoids with low TiO_2 concentrations. The presence of abundant olivine and pyroxene phenocrysts (up to 30 vol %) determines the porphyritic textures of the rocks and their melanocratic composition, whereas their leucocratic groundmass contains feldspars and analcime. The reported K–Ar ages of the subvolcanic bodies at mounts Khukhch and Emguchan' point to their Middle–Late Miocene age of 8–17 Ma (Koval' and Adamchuk, 1986). Based on newly obtained data, the trachybasalts of Mount Khukhch were classed with basanites.

The basanites of Mount Khukhch (triangulation height 306.5 m on the right-hand side of the Bystraya River, near the mouth of the Khukhch River and the upper reaches of the Chananka River) compose a small (60–80 m^2) stock or a fragment of a large dike among other subvolcanic bodies of subalkaline and alkaline basaltoids widespread in the area (Fig. 1). The subvolcanic basanite body is hosted by a volcanic–sedimentary sequence of the undifferentiated Viventekskaya and Kuluvenskaya formations of Late Oligocene–Early Miocene age (Gladenkov et al., 1998), which are members of the Middle Eocene–Early Miocene Vayampol'skaya Group, and has intrusive contacts with these rocks. The formations are composed of tuffites, tuffs, tuff–siltstones, and tuff–mudstones. In the regional geological sense, the area including the subvolcanic basanite bodies is restricted to the southwestern closure of a large northeast-trending depression filled with Oligocene–Miocene deposits. The depression rests on a volcanic–sedimentary Cretaceous–Paleogene basement, and its eastern limb is overlain by Neogene–Quaternary complexes of the volcanic belt of the Sredinnyi Range.

According to the geological–geophysical data in (Antipov et al., 1997), the deposits of the Viventekskaya and Kuluvenskaya formations belong to the upper levels of a large seismo-stratigraphic complex, which is recognized in the sedimentary sequences of the Sea of Okhotsk and western Kamchatka. The formation of this complex was associated with high-amplitude tectonic motions.

ANALYTICAL TECHNIQUES

The concentrations of major oxides in basanites were determined on a SRM-25 (Russia) multicollector X-ray spectrometer, with Fe_2O_3 and FeO distinguished by titration. The concentrations of trace elements in the samples were analyzed by ICP-MS.

The ICP-MS analyses of two basanite samples for trace elements were conducted with two methods of sample preparation and on two mass spectrometers of various accuracy classes. At the Institute of the Earth's Crust, the samples were decomposed using microwaves: 50-mg samples were placed into a tetrafuorethylene (Teflon) container and decomposed by a mixture of HF and HNO_3 (in the proportion 3 : 1, doubly distilled acids of reagent purity grade) in a microwave oven. The resultant solution was evaporated in a glassy carbon vessel. For more complete decomposition and silica removal, the sample was then again evaporated with HF and, upon addition of HNO_3, H_2O_2, and H_2O, evaporated again. This method of sample preparation was described in detail in (Yasnygina et al., 2003).

At the Vinogradov Institute of Geochemistry, the samples were decomposed in open systems. Samples 100 mg in mass were placed into tetrafuorethylene (Teflon) vials together with a mixture of acids (5 ml of reagent-grade HF, 2 ml of doubly distilled reagent-grade HNO_3, and 1 ml of superior-class $HClO_4$) and left overnight at room temperature. After that, the content of the vessel was evaporated to get rid of SiF_4, and 1 ml of H_2O, 1 ml of HNO_3, and 2–3 drops of H_2O_2 were added to the residue. The mixture was held again for 12 h and then evaporated to insipient dryness, placed into a 100-ml flask, and the flask was then line-filled with water. The water used in both techniques was purified on Millipore ELIX-3 (France).

The measurements were conducted on a Plasma Quad 2+ (VG Elemental, England) quadrupole mass spectrometer and on an ELEMENT 2 (Finnigan MAT, Germany) magnetic sector mass spectrometer. The ELEMENT 2 mass spectrometer is characterized by double focusing and allows recording signal in three resolution modes: low (LR)—300, medium (MR)—4000, and high (HR)—10000 M/ΔM. The resolution of the Plasma Quad 2+ mass spectrometer corresponds to LR ~ 300 M/ΔM. The analysis was carried out under standard operation conditions of the corresponding mass spectrometers: see (Ivanov et al., 2000) for Plasma Quad 2+ and (Smirnova et al., 2004) for ELEMENT 2. In order to minimize the possible matrix effect and signal fluctuations, the spectra were taken with the use of internal standards; ^{115}In and ^{209}Bi (10 ng/ml for each in the ready solution) for Plasma Quad 2+ and ^{103}Rh (2 ng/ml) for ELEMENT 2. The spectral interference was reduced by selecting the analytical isotopes free of mass interferences or, if this procedure was not possible, by correcting the intensities of the signals (for example, for ^{151}Eu and ^{159}Tb). In addition, analyses on ELEMENT 2 were conducted in LR

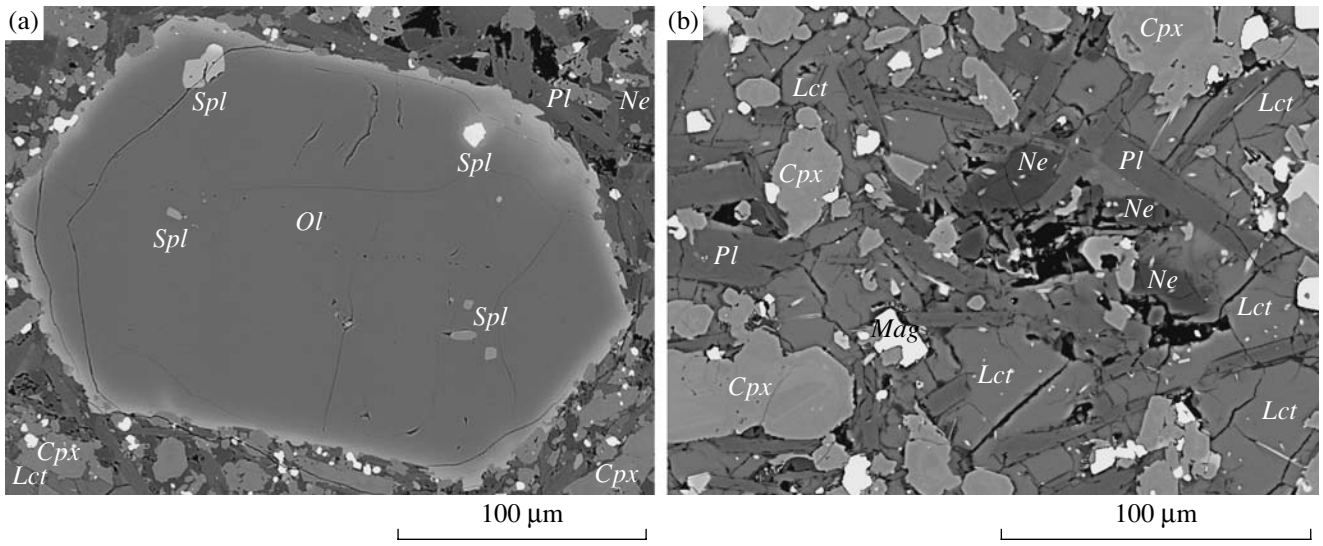

Fig. 2. Textures and mineral assemblages of basanites from Mount Khukhch, western Kamchatka.
(a) Porphyritic texture of the basanite: euhedral olivine (*Ol*) phenocryst with spinel (*Spl*) inclusions in a microdoleritic groundmass; (b) basanite groundmass: plagioclase (*Pl*) laths and microlites, microlites of clinopyroxene (*Cpx*) and titanomagnetite (*Mag*), interstitial nepheline (*Ne*) and leucite (*Lct*). Back-scattered electron images (taken on a LEO 1430VP scanning electron microscope, Geological Institute, Siberian Division, Russian Academy of Sciences, operator N.S. Karmanov).

and/or MR resolution modes, which permitted us to distinguish between the masses of interfering isotopes. The dependences of intensities on element concentrations during ELEMENT 2 analyses were calibrated against multielemental standard certified solutions (CLMS-1-4 and SPEX, United States). The dependences for Plasma Quad 2+ were calibrated on standard reference samples (BIR-1, DNC-1, BHVO-1, BCR-2, JB-2, RGM-1, AGV-1, and STM-1). The solutions of the samples prepared for analysis were 1000-fold (for Plasma Quad 2+) and 5000-fold (for ELEMENT 2) diluted at acidity of 2% HNO_3.

The detection limits (DL) were assayed by the 3σ criterion for the total blank and recalculated to the solid sample at the corresponding dilution factor of the solutions. These parameters were varied depending on the "purity" of the blank sample and the dilution of the solutions. In the actual analyses, the DL values for elements were from 1 to 0.00*n* ppm for Plasma Quad 2+ and from 0.1 to 0.001 ppm for ELEMENT 2; the DL for REE did not exceed 0.0*n* ppm, which is much lower than the concentrations of these elements in our samples. The standard deviations, which were evaluated from replicate measurements in standards (whose trace-element concentrations were close to those in the samples) varied from 0.3–0.8% (Sr, Zr, Cs, Nd, and La) to 7–8% (Cr, Zn, and Tm). The accuracy of the analyses was controlled using internationally certified standards of basalts (BIR-1, BHVO-1, JB-2, and BCR-2), dolerite (DNC-1), rhyolite (RGM-1), and andesite (AGV-1).

The concentrations of trace elements in the samples of volcanic rocks obtained by the two aforementioned methods on two ICP-MS mass spectrometers of various accuracy classes were comparable.

The Sr isotopic composition ($^{87}Sr/^{86}Sr$) was measured on a MI-1201T mass spectrometer in single-filament mode, with the use of a Ta emitter (operator Yu.A. Pakhol'chenko).

Minerals were analyzed on a Camebax 244 X-ray spectral microprobe at the Institute of Volcanology and Seismology, Far East Division, Russian Academy of Sciences, under the following operation conditions: accelerating voltage of 20 kV, sample current 40 nA, counting time 5 s, K_α analytical lines. The standards were from the collection of mineral standards of the Far East Geological Institute, Far East Division, Russian Academy of Sciences (sanidine, olivine, ilmenite, diopside, rhodonite, spinel, and zincite).

PETROGRAPHY AND MINERALOGY OF BASANITES

The basanites are massive rocks of grayish black and dark gray to black color. The rocks are relatively fresh, and their insignificant secondary alterations involve thin films of Fe hydroxides around crystals of mafic minerals. The microphyric texture of the basanites is defined by the presence of numerous euhedral and resorbed olivine phenocrysts (Fig. 2a) and rare clinopyroxene phenocrysts in a fine-grained microdoleritic groundmass. Olivine phenocrysts are dark yellow and greenish yellow, elongated-prismatic, rounded, or angular, and their sizes mostly range from 0.4 to 0.7 mm, occasionally reaching 1.5–2 mm. Even larger sizes, up to 6–7 mm in length, are typical of single pris-

matic olivine crystals. The content of olivine phenocrysts amounts to 18–20 vol % of the rock. They are typically surrounded by well-developed iddingsite rims and bear minute inclusions of spinel in the cores and marginal zones. Most olivine crystals show trace of melting, which resulted in rounded grains and those with rounded faces and embayed with the groundmass material. Olivine occurs in the basanites not only as phenocrysts but also as smaller subphenocrysts and microlites. The rocks occasionally bear aggregates of olivine and clinopyroxene subphenocrysts. Single clinopyroxene phenocrysts of brownish-black color in hand-specimens and pale brown in thin sections have sizes of up to 0.7–1.2 mm. Along with plagioclase and titanomagnetite, clinopyroxene is much more abundant as subphenocrysts (0.2–0.3 mm) and microlites. The basanites contain rare lenticular and equant aggregates of clinopyroxene crystals up to 5–6 mm across.

The microdoleritic groundmass of the basanites contains two successively crystallizing microlite populations and interstitial minerals. The earliest population of microlites comprises laths (subphenocrysts) of plagioclase, euhedral prismatic and anhedral plagioclase and clinopyroxene microlites, and titanomagnetite grains (Fig. 2b). The plagioclase laths reach sizes of 20×100 μm and are randomly oriented. Plagioclase laths are in aggregates in clinopyroxene microlites, whose average sizes are 20×50 μm (occasionally 50×100 μm), and rare titanomagnetite. It should be mentioned that clinopyroxene crystals, on the one hand, and plagioclase laths, on the other, compose equant aggregates, which determine the unclearly pronounced mosaic heterogeneity of the groundmass. The rocks commonly contain aggregates of titanomagnetite grains and clinopyroxene microlites, which testifies to the concurrent crystallization of these minerals. The latest crystallization phase of the basanites is represented by groundmass microlites and interstitial grains of nepheline, leucite, and rare sodic plagioclase (the grains have sizes of 5×20, 20×30 μm and less). The sodic plagioclase composes much smaller euhedral grains than the feldspar laths and microlites. Another rare interstitial phase is analcime. Nepheline and leucite compose interstitial zones between plagioclase laths and clinopyroxene microlites in the groundmass. Feldspathoid crystals rarely show poorly pronounced crystal faceting and have short-prismatic, triangular, or, even more rarely, polygonal cross sections. Nepheline grains sometimes show mosaic extinction and fine concentric zoning. However, the morphology of nepheline and leucite grains is controlled mostly by that of the interstitial space. The relations observed between feldspathoids, when leucite crystals in interstices are surrounded by nepheline or are in aggregates with it, suggest that the minerals crystallized simultaneously. The groundmass contains abundant thin acicular apatite crystals. Their position relative to other microlites and interstitial mineral grains suggests that the apatite crystallized after plagioclase laths and clinopyroxene and titanomagnetite microlites.

The average assayed volumetric proportions of mineral phases in the basanites are as follows (petrographic–mineralogical counting data): ~22% olivine phenocrysts, subphenocrysts, and microlites; ~34% clinopyroxene subphenocrysts and microlites; ~21% plagioclase; and ~4% titanomagnetite. The proportions of microlites and interstitial phases are as follows: ~16% nepheline, ~3% leucite, and <1% analcime and apatite (the consistency of the rock composition and the proportions of its mineral phases was confirmed by balance calculations). For the final crystallization stage of the basanites, the residual melt fraction was assayed at ~58%.

Petrographic observations imply the following crystallization sequence of mineral assemblages in the basanite melt. The earliest subliquidus phases were spinel and olivine. Spinel inclusions in the cores of olivine phenocrysts and then in their marginal zones suggest their concurrent crystallization. Upon the termination of olivine phenocryst crystallization and the crystallization of rare clinopyroxene phenocrysts, the crystallization conditions of the basanite melt notably changed. Olivine crystals started to melt and were resorbed, perhaps, because of temperature and, mostly, pressure changes during the rapid ascent of the melt. The melt then likely started to crystallize in situ, when the magmatic reservoir was formed. Melt crystallization during this stage resulted in the *Pl–Cpx–TiMag* microlite assemblage with minor amounts of olivine and apatite. During the final stage, the residual melt rich in alkalis started to crystallize microlites of sodic plagioclase and interstitial leucite, nepheline, and rare analcime.

The compositional evolution of minerals in the basanites from phenocrysts to microlites reflects the generally typical successive crystallization of magnesian melts of basic composition with an evolution from more melanocratic to more leucocratic mineral assemblages, an increase in the fe# of olivine, Ti content in ore minerals and pyroxenes, and alkali concentrations in aluminosilicates.

Spinel inclusions in the cores of olivine phenocrysts are compositionally close to picotite and Cr-picotite: Al_2O_3 32.9–46.2 wt %, Cr_2O_3 13.5–19.2 wt %, MgO 10.1–16.7 wt %, f = 59.3–78.1 (Table 1, Fig. 3a).[1] Spinel in intermediate olivine zones becomes more ferrous (f = 85.3) and less aluminous (23.8 wt % Al_2O_3) and magnesian (8.1 wt % MgO). In zonal olivine crystals, the boundaries between their forsterite cores and hortonolite margins are marked by the presence of spinel of transitional composition, lower concentrations of Al_2O_3 (8.3 wt %), Cr_2O_3 (4.3 wt %), and MgO (3.7 wt %) and with high concentrations of TiO_2 (16.1 wt %). The ore mineral in aggregates with olivine

[1] f is the iron mole fraction (Table 1).

Table 1. Compositions (wt %) of spinel and olivine in basanites from western Kamchatka

Component	Spinels				Olivine						
	inc-c	inc-i	inc-m	mcl	phc-c	phc-i	phc-m	sphc-c	sphc-m	mcl-c	mcl-m
SiO_2	0.04	0.00	2.07	0.00	41.41	39.67	37.10	38.92	37.29	36.69	35.44
TiO_2	1.65	16.15	18.84	22.26	0.00	0.00	0.09	0.00	0.03	0.03	0.04
Al_2O_3	40.34	8.25	4.42	1.87	0.00	0.01	0.00	0.00	0.00	0.00	0.00
Cr_2O_3	16.15	4.34	1.52	0.09	0.00	0.02	0.00	0.00	0.00	0.00	0.00
Fe_2O_3	10.87	24.33	22.78	23.50	0.00	0.30	0.35	0.01	0.27	0.49	0.20
FeO	18.48	40.57	44.44	46.71	11.75	15.79	30.14	16.91	28.40	30.22	37.51
MnO	0.12	0.58	0.64	0.62	0.10	0.10	0.61	0.20	0.61	0.64	0.97
MgO	14.07	3.76	4.03	2.27	46.87	43.67	31.73	41.97	33.24	31.28	24.99
CaO	0.00	0.00	0.05	0.23	0.05	0.19	0.51	0.16	0.45	0.56	0.62
Na_2O	0.00	0.00	0.00	0.00	0.00	0.00	0.00	0.00	0.00	0.00	0.00
K_2O	0.05	0.00	0.14	0.07	0.00	0.03	0.02	0.00	0.03	0.00	0.03
Total	101.78	97.98	98.96	97.63	100.17	99.78	100.55	98.18	100.33	99.91	99.81
Fo (*f*)	66.45	94.35	94.20	96.78	87.58	82.79	64.52	81.37	66.96	64.04	53.53
Fa					12.31	17.10	34.77	18.41	32.35	35.21	45.29
Tp					0.11	0.11	0.71	0.22	0.69	0.75	1.18
n	9	1	3	7	4	9	5	3	3	5	5

Note: Average compositions of minerals are reported, *n* is the number of analyses for which the averages were calculated. Phases: **inc-c** and **inc-i** are spinel inclusions in the cores and intermediate zones of olivine phenocrysts, **inc-m** are magnetite inclusions in the marginal zones of olivine phenocrysts and magnetite in aggregates with olivine; **mcl**—microlites (**mcl-c** and **mcl-m** are the cores and margins of microlites), **phc-c**, **pcr-i**, and **phc-m** are the cores, intermediate zones, and margins of phenocrysts; **sphc-c**, **sphc-i**, and **sphc-m** are the cores, intermediate zones, and margins of subphenocrysts. Here and below, Fe_2O_3 was calculated from stoichiometric considerations; *Fo*—forsterite, *Fa*—fayalite, *Tp*—tephroite (mol %). The iron mole fraction was calculated as $f = (FeO_{tot} + MnO)/(FeO_{tot} + MnO + MgO)$.

in contact with the rock groundmass is titanomagnetite ($f = 93.8–94.4$): Al_2O_3 2.4–2.5 wt %, Cr_2O_3 0.1 wt %, MgO 3.9–4.3 wt %. This mineral is notably more magnesian than magnetite microlites in the groundmass of the basanites (Al_2O_3 1.5–2.3 wt %, MgO 1.5–2.7 wt %, $f = 96.1–97.8$). The TiO_2 concentrations in the ore minerals systematically increases from spinel in inclusions in the cores of olivine grains (TiO_2 0.9–2.7 wt %) to inclusions in the marginal portions of the grains (4.86 wt % TiO_2) and then drastically increases in titanomagnetite in its aggregates with olivine (19.6–20.7 wt %) and further to titanomagnetite microlites in the groundmass (20.0–25.1 wt %) (Table 1, Fig. 3a). The minor components of the spinels in inclusions in olivine are NiO (up to 0.26 wt %) and, in magnetite microlites, V_2O_5 (qualitatively identified elevated concentrations).

Olivine in the basanites evolves from forsterite in the cores and intermediate zones of phenocrysts to hortonolite in their margins and further increases its fe# in subphenocrysts and microlites (Table 1, Fig. 3b). The olivine shows three discrete compositional ranges, which correspond to the crystallization stages of this mineral. The compositional variations from the cores ($Fo_{88.1–83.1}$) to intermediate zones of olivine phenocrysts ($Fo_{84.0–79.4}$) are relatively insignificant, and the crystals are only weakly zonal. The compositions of the intermediate zones of olivine phenocrysts correspond to the compositions of the cores of subphenocrysts ($Fo_{82.3–80.4}$). Another discrete compositional range of olivine corresponds to the margins of phenocrysts ($Fo_{72, 69.6–62.8}$) and subphenocrysts ($Fo_{69.2–66.4}$) and the cores of microlites ($Fo_{65.4–64.4}$). Finally, the third, final phase of olivine crystallization corresponds to the compositions of the outer zones of olivine microlites with the maximum fe# ($Fa_{42.3–47.8}$). The compositional ranges of olivine are also characterized by a systematic increase in the CaO concentrations from phenocrysts to subphenocrysts and then to microlites: 0.05–0.19, 0.16–0.45, and 0.56–0.62 wt % on average, respectively. The discrete ranges of olivine composition in the basanites correspond to the following stages: (1) crystallization of olivine phenocrysts and the onset of crystallization of subphenocrysts, (2) termination of the crystallization of phenocrysts and the beginning of formation of microlites, and (3) termination of the crystallization of microlites. It should be mentioned that the cores of olivine phenocrysts include the most magnesian compositions ($Fo_{88.1–87.8}$) with the lowest CaO concentrations (0.00–0.06 wt %). The genesis of this mineral phase can be considered from the viewpoint of its

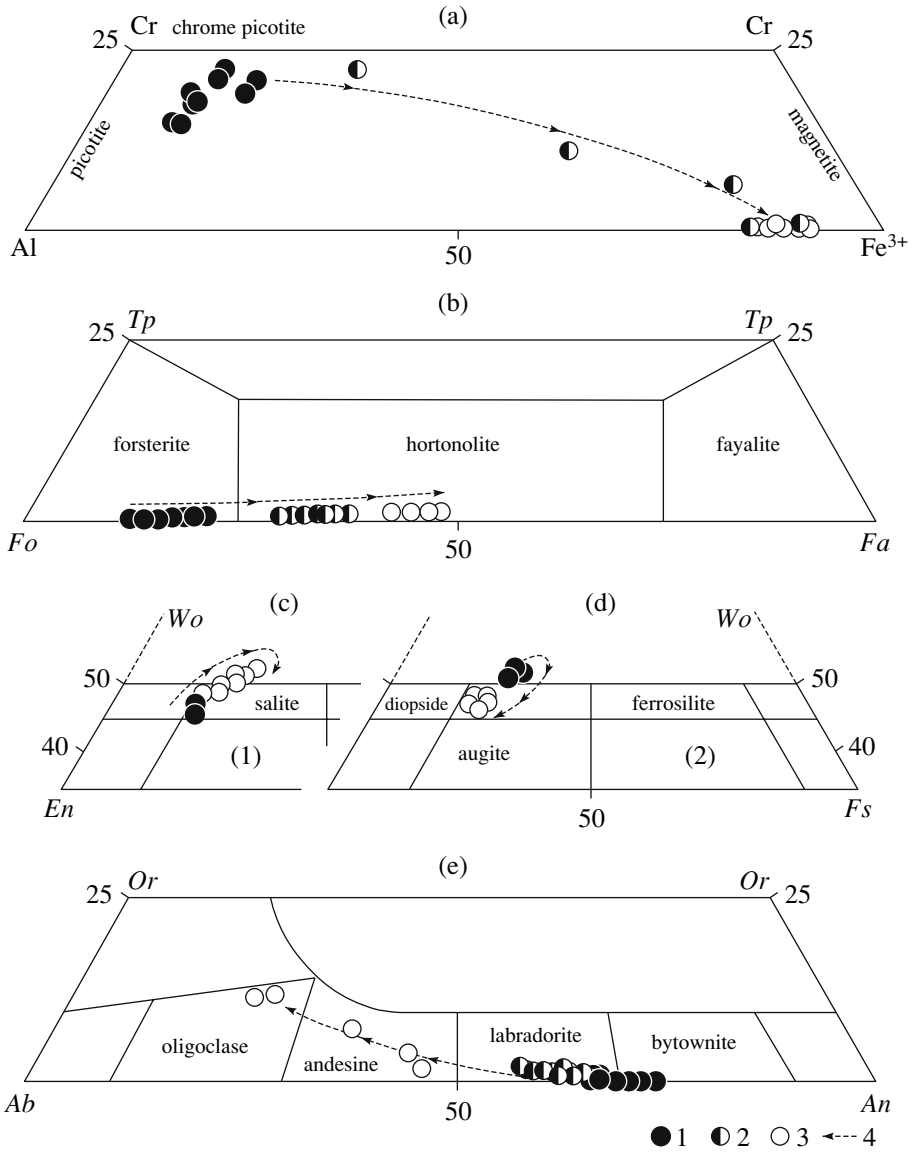

Fig. 3. Classification compositional diagrams for (a) spinels, (b) olivine, (c) clinopyroxene, and (d) plagioclase in basanites from western Kamchatka.

(a) (1) Spinel of inclusions in the cores of olivine phenocrysts; (2) spinel of inclusions in the marginal zones of olivine phenocrysts and titanomagnetite in aggregates with olivine; (3) titanomagnetite microlites in the groundmass.

(b) (1) Cores and intermediate zones of phenocrysts and the cores of subphenocrysts of olivine; (2) marginal zones of phenocrysts and subphenocrysts and the cores of microlites of olivine; (3) marginal zones of olivine microlites.

(c) (1) Cores of clinopyroxene phenocrysts; (3) marginal zones of clinopyroxene phenocrysts and clinopyroxene subphenocrysts.

(d) (1) Cores of clinopyroxene microlites; (2) marginal zones of clinopyroxene microlites.

(e) Plagioclase populations arranged in decreasing order of their size: (1) plagioclase laths; (2) plagioclase microlites; (3) sodic plagioclase microlites; (4) compositional trend of minerals during the successive crystallization of phases.

crystallization in equilibrium with the primary or parental basanite melt and under the assumption of its xenogenic, mantle origin.

The clinopyroxene of the basanites shows unusual (but expectable, as will be shown below) compositional evolution (Table 2, Figs. 3c, 3d). The mineral is salite and fassaite, which are clinopyroxene with isomorphism according to the scheme $Si^{+4} + Mg^{+2} \longleftrightarrow Al^{+3} + Ti^{+3}$. The cores of rare clinopyroxene phenocrysts correspond to salite ($Wo_{46.0–47.8}Fs_{10.2–10.7}$) and give way to fassaite compositions of intermediate zones ($Wo_{48.7–49.6}Fs_{10.1–12.5}$) with weak zoning expressed as an increase in the concentrations of TiO_2, Al_2O_3, and the *Wo* end member. The further crystallization of the mineral (transition from the marginal of its phenocrysts and subphenocrysts to the cores of its microlites) is marked

Table 2. Compositions (wt %) of plagioclase and clinopyroxene in basanites from western Kamchatka

Component	Plagioclase			Clinopyroxene							
	laths	mcl	mcl	phc-c	phc-i	phc-i	phc-i	phc-m	phc-m	mcl-c	mcl-m
SiO_2	49.04	50.81	57.86	52.29	48.43	44.49	41.03	43.39	48.31	41.55	47.12
TiO_2	0.08	0.15	0.09	0.73	1.98	2.77	4.28	3.37	2.02	4.05	2.08
Al_2O_3	31.85	30.48	25.60	3.88	6.58	9.74	11.97	10.19	6.54	11.24	6.36
Cr_2O_3	0.00	0.00	0.00	0.00	0.05	0.00	0.00	0.00	0.00	0.00	0.00
FeO*	0.73	0.88	0.52	6.46	6.82	7.93	8.70	8.23	7.31	8.49	7.51
MnO	0.00	0.00	0.00	0.03	0.00	0.00	0.01	0.00	0.04	0.01	0.01
MgO	0.06	0.04	0.03	14.73	13.46	11.69	10.23	11.27	13.04	10.72	13.35
CaO	14.51	12.88	7.05	22.55	23.29	23.23	23.04	22.99	22.87	22.98	22.66
Na_2O	3.41	4.25	6.23	0.51	0.41	0.48	0.29	0.36	0.31	0.37	0.28
K_2O	0.00	0.26	1.62	0.00	0.00	0.00	0.00	0.00	0.00	0.00	0.00
Total	99.67	99.74	98.99	101.18	101.02	100.33	99.55	99.80	100.44	99.41	99.37
An (*Wo*)	70.19	61.76	34.69	46.88	49.17	50.81	52.24	50.94	48.94	51.56	48.09
Ab (*En*)	29.81	36.78	55.90	42.62	39.53	35.57	32.27	34.74	38.82	33.47	39.41
Or (*Fs*)	0.00	1.46	9.41	10.50	11.30	13.62	15.49	14.32	12.24	14.97	12.50
n	8	10	6	2	2	1	1	1	1	5	7

Note: *An*—anorthite, *Ab*—albite, *Or*—orthoclase, *Wo*—wollastonite, *En*—enstatite, *Fs*—ferrosilite; FeO*—all Fe calculated as FeO. See Table 1 for other explanations.

Table 3. Compositions (wt %) of interstitial feldspathoids and analcime in basanites from western Kamchatka and the groundmass of the rocks

Component	Leucite		Nepheline		Analcime		Groundmass			
	gm*	gm	gm*	gm	gm	gm	rastering over areas of 50 × 50 and 100 × 100 μm			
SiO_2	55.23	55.50	49.34	48.46	47.25	48.68	45.86	47.34	47.75	47.92
TiO_2	0.04	0.04	0.03	0.05	0.04	0.05	2.40	1.50	1.80	1.59
Al_2O_3	23.75	23.21	31.37	30.99	29.82	30.39	19.51	19.46	20.59	21.72
Cr_2O_3	0.00	0.00	0.01	0.00	0.00	0.00	0.00	0.00	0.00	0.00
FeO*	0.52	0.41	0.64	0.63	0.73	0.78	8.91	4.79	6.16	5.35
MnO	0.00	0.00	0.00	0.00	0.00	0.00	0.00	0.00	0.00	0.11
MgO	0.02	0.02	0.04	0.03	0.03	0.04	4.58	4.99	3.82	3.30
CaO	0.14	0.29	0.92	0.86	0.57	0.56	10.00	12.20	10.21	9.96
Na_2O	0.19	0.07	14.69	14.65	11.54	9.31	6.44	7.32	6.34	6.54
K_2O	21.16	20.77	2.68	2.76	2.45	2.44	3.30	1.71	2.80	2.43
H_2O					8.05	8.14				
Total	101.05	100.31	99.71	98.43	100.48	100.39	101.00	99.30	99.47	98.92
n	3	3	7	4	1	1	3	2	7	13

Note: For the compositions of leucite and nepheline, gm*—sample PP-2264, gm—sample PP-2265. See Table 1 for other explanations.

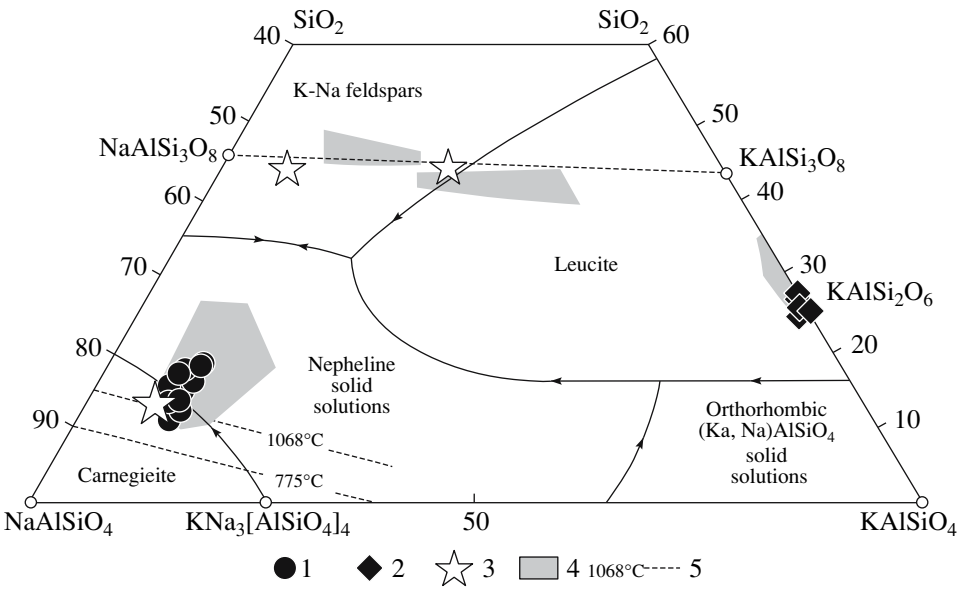

Fig. 4. $NaAlSiO_4$–$KAlSiO_4$–SiO_2 diagram (Schairer, 1950) for the interstitial feldspathoids in basanites from western Kamchatka. (1) Interstitial nepheline in basanites from western Kamchatka; (2) interstitial leucite in basanites from western Kamchatka; (3) feldspar and nepheline microlites in Miocene basanites from eastern Kamchatka (Volynets et al., 1997); (4) interstitial K–Na feldspar, nepheline, and leucite in Quaternary basalts of the alkaline olivine basalt series in the Sredinnyi Range, Kamchatka (Volynets and Anan'ev, 1984); (5) solubility limits of the nepheline solid solution under anhydrous conditions (T = 1068°C) and under P_{H_2O} = 1 kbar (T = 775°C) (Deer et al., 1965). Solid lines correspond to the boundaries of the compositional fields of crystalline phases and solid solutions, arrows indicate decreasing crystallization temperatures.

by a definite enrichment in fassaite (within the range of $Wo_{50.1–52.2}Fs_{13.3–15.5}$). The clinopyroxene thereby becomes enriched in TiO_2 and Al_2O_3 (to 4.2 and 12.0 wt %, respectively). After the growth of the marginal zones of clinopyroxene microlites, the compositional evolution of the minerals changes to the opposite one: from fassaite to salite, with a drastic decrease in the concentrations of the wollastonite end member and TiO_2 (to $Wo_{47.4–48.6}Fs_{11.7–13.4}$ and TiO_2 1.8–2.3 wt %). The possible reason for this could be the depletion of the residual melt in TiO_2 as a consequence of the massive crystallization of titanomagnetite microlites. Note that the compositional evolution of the clinopyroxene from the cores of its phenocrysts to their marginal zones is characterized by a significant decrease in the Na_2O concentration: from 0.50–0.51 to 0.29–0.31 wt %.

The only feldspar of the basanites is plagioclase. Subphenocrysts (laths) of plagioclase consist of K-free bytownite and labradorite ($An_{74–66}Or_0$) with a weak decrease in the content of the albite end member toward the margins of the crystals (Table 2, Fig. 3e). Small plagioclase microlites of tabular morphology (<50 μm) have a labradorite composition and contain notable K_2O concentrations ($An_{67–57}Or_{1.1–2.1}$), and the most sodic plagioclase of andesine and oligoclase composition ($An_{50–21}Or_{4–12}$) composes microlites in association with interstitial nepheline and leucite.

The nepheline filling the interstitial space in the groundmass of the basanites shows persistent compositional variations and corresponds to carnegieite and nepheline solid solution (Table 3). The compositional data points of the nepheline group near the equilibrium line of the phases in the $NaAlSiO_4$–$KAlSiO_4$–SiO_2 feldspathic join (Fig. 4). The composition of nepheline from the western Kamchatkan basanites is noted for elevated contents of SiO_2, K_2O, and, to a lesser degree, also CaO and FeO. Similar compositional characteristics were shown by nepheline in alkaline basaltoids in other areas in Kamchatka (Volynets and Anan'ev, 1984) and are considered typical of nepheline and leucite in volcanic rocks. The interstitial leucite of the basanites is close to its idealized formula composition with minor admixtures of Na_2O, CaO, and FeO (Table 3, Fig. 4).

The identified interstitial phases of the basanites include hydrous K–Na aluminosilicates, which were provisionally assumed to be analcime. This mineral crystallizes late in the crystallization course of basanites. The composition of the analcime notably differs from its idealized formula in having lower SiO_2 and higher Al_2O_3 concentrations, and compared to this mineral in magmatic rocks elsewhere in Kamchatka, our analcime is higher in K_2O (Volynets et al., 1985, 1997; Flerov et al., 1998). The analcime and nepheline show similar balance of components, except lower Na_2O in the former. High-K analcime was previously described in the literature (Deer et al., 1965), along with experimentally synthesized compositions identified as hydronepheline containing 8.9 wt % H_2O (Yakubovich and Tarasov, 1988). H_2O molecules in the hydronepheline

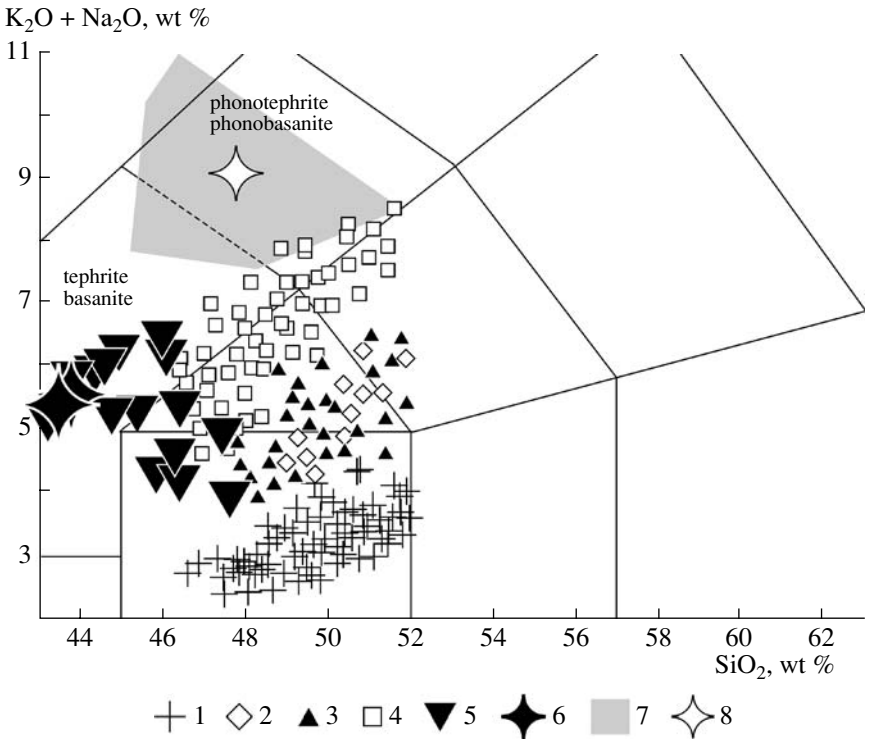

Fig. 5. SiO_2–($K_2O + Na_2O$) classification diagram for the Mount Khukhch basanites and basaltoids of various geodynamic types from other areas in Kamchatka (LeBas et al., 1986).

(1) Island-arc moderate-K basalts of Neogene–Quaternary volcanic belts in Kamchatka; (2) island-arc high-K and shoshonitic basalts of the Neogene–Quaternary volcanic belt in the Sredinnyi Range; (3) Pliocene–Quaternary basalts of the K–Na alkaline basaltic and alkaline olivine basaltic series in the Sredinnyi Range; (4) basaltoids of the potassic alkaline and subalkaline series in western Kamchatka (absarokites, trachybasalts, and shonkinites); (5) basaltoids of the K–Na alkaline and subalkaline series in eastern Kamchatka; (6) basanites of Mount Khukhch, western Kamchatka; (7) compositional field of the Mount Khukhch basanites; (8) average composition of the Mount Khukhch basanites. The diagram is based on our and literature data.

structure partly substitute Na in the voids of the aluminosilicate framework, i.e., occupy sites analogous to those in zeolites.

The compositional trend of the residual basanite melt during the crystallization of olivine phenocrysts in assemblage with spinel and magnetite and the subsequent massive crystallization of olivine, plagioclase, clinopyroxene, and titanomagnetite subphenocrysts and microlites can be revealed by microprobe rastering analyses of the groundmass of these rocks. The raster analyses over areas of 50×50 and 100×100 μm significantly vary in concentrations of several components, perhaps, because the rastering areas were comparable in size with microlites. This problem was solved by the stepwise shift of the rastering areas. The analyses generally display an increase in alkali and alumina contents in the process of its crystallization up to the appearance of phono-tephrite compositions (Table 3, Fig. 5).

GEOCHEMISTRY OF THE BASANITES

The basanites of Mount Khukhch belong to the group of basic feldspathoid-bearing alkaline rocks of the K–Na series ($Na_2O/K_2O = 1.5$–1.9). The contents of normative nepheline are 13–14 wt % and those of olivine are 21–22 wt %. The rocks are noted for elevated concentrations of MgO, TiO_2, Na_2O, and K_2O (Table 4). Compared to basaltoids of other geochemical types found in the magmatic areas of the Kamchatkan arc system, the Mount Khukhch basanites and the basanites and alkaline basaltoids from eastern Kamchatka show the highest total alkalinity and low silicity (Fig. 5). The basanites are characterized by high concentrations of compatible siderophile elements (Co, Ni, and Cr), HFSE (Nb and Ta), radioactive elements (Th and U), and LREE at moderate concentrations of Zr, Hf, alkaline, alkali-earth, and trace chalcophile elements (Rb, Ba, Sr, Pb, Cu, ad Sn). The rocks exhibit highly fractionated REE patterns (La_N/Yb_N = 10.8–12.6), and many of their indicator trace elemental ratios (Ba/Nb = 10–12, Sr/Nb = 17–18, Ta/Yb = 1.3–1.6) suggest that the basanites in western Kamchatka affiliate with the group of basaltoids of the within-plate geochemical type. This is clearly illustrated by the Ba/Zr–Nb/Zr diagram (Fig. 6), in which the compositional data points of the basanites cluster along the compositional trend for basaltoids of mid-oceanic ridges (MORB) and within-plate environments. The

Table 4. Concentrations of major (wt %) and trace (ppm) elements in basanites from Mount Khukhch, western Kamchatka

Component	PP-2264	PP-2265	Component	PP-2264	PP-2265	Component	PP-2264	PP-2265
SiO_2	43.52	43.80	Rb	41	42	U	1.51	1.48
TiO_2	1.96	1.96	Ba	557	558	La	34.50	34.22
Al_2O_3	14.39	14.55	Sr	890	890	Ce	73.63	72.10
Fe_2O_3	4.73	4.79	Pb	2.99	2.80	Pr	9.09	8.80
FeO	7.18	7.00	Zn	76	72	Nd	33.04	32.44
MnO	0.18	0.17	Cu	42	44	Sm	6.79	6.64
MgO	10.96	11.00	Co	51	50	Eu	1.96	1.89
CaO	9.75	9.89	Ni	245	232	Gd	6.13	6.55
Na_2O	3.30	3.56	Cr	356	343	Tb	0.82	0.96
K_2O	2.11	1.90	V	249	239	Dy	4.56	4.69
P_2O_5	0.67	0.65	Sc	25	30	Ho	0.84	0.93
H_2O	0.80	0.55	Ta	2.90	2.79	Er	2.31	2.31
CO_2	0.23	0.17	Nb	51.0	49.1	Tm	0.29	0.31
Total	99.78	99.99	Zr	167	192	Yb	1.86	2.15
F	440	700	Hf	4.06	4.11	Lu	0.25	0.27
Cs	0.56	0.55	Th	4.43	4.44	Y	21	23

Note: Major oxides were determined by XRF, Fe was analyzed by titration, F and CO_2 were determined by conventional chemical techniques (at the Vinogradov Institute of Geochemistry, Siberian Division, Russian Academy of Sciences, analysts A.K. Klimova, L.P. Koval', G.A. Pogudina, and T.V. Ozhogina). The concentrations of trace elements were determined by ICP-MS at the Analytical Center for Collective Use of the Irkutsk Research Center, Siberian Division, Russian Academy of Sciences: sample PP-2264 was analyzed on an ELEMENT 2 high-resolution mass spectrometer (Vinogradov Institute of Geochemistry, Siberian Division, Russian Academy of Sciences, analysts L.A. Chuvashova, E.V. Smirnova, and V.I. Lozhkin), sample PP-2265 was analyzed on a VG Plasma Quad 2+ quadrupole mass spectrometer (Institute of the Earth's Crust, Siberian Division, Russian Academy of Sciences, analysts M.E. Markova and T.A. Yasnygina).

concentration levels of trace elements and the ranges of trace-element ratios for the western Kamchatkan basanites coincide with those for alkaline basaltoids in eastern Kamchatka, for example, Ba/Nb = 6–15 and Sr/Nb = 10–29. At the same time, the comparison of the composition of the Mount Khukhch basanites and the K–Na alkaline and subalkaline Pliocene–Quaternary basaltoids from the Sredinnyi Range, which are considered to be another example of within-plate magmatic products in the territory of the Kamchatkan arc system (Volynets, 1993, 1994; Churikova et al., 2001; Ivanov et al., 2004), demonstrates their notable compositional differences. Starting with their nepheline-normative members (Ba/Nb = 15–30, Sr/Nb = 27–73) to hypersthene- and olivine-normative transitional types (Ba/Nb = 25–75, Sr/Nb = 41–86), the basaltoids of the alkaline olivine basaltic and alkaline basaltic series in the Sredinnyi Range define an intermediate trend between the compositional fields of rocks of within-plate and island-arc geochemical types (Ba/Nb = 109–250, Sr/Nb = 108–441). Thereby even the compositions of nepheline-normative basalts from the Sredinnyi Range, which are the most strongly enriched in HFSE, deviate from the compositional trend of typical within-plate magmas toward basaltoids of the island-arc type (in contrast to the alkaline basaltoids of western and eastern Kamchatka). This comparison is important for distinguishing not only rocks of the within-plate and arc geochemical types among the magmatic rocks of the Kamchatkan arc system but also of an extensive group of transitional series.

In multielemental diagrams for elements characterized by various affinity to magmatic melts, the compositional features of various basaltoid types from the Kamchatkan arc system are pronounced even more clearly (Fig. 7). The basanites from western Kamchatka are characterized by plots of the distributions of trace elements similar to those of basanites from eastern Kamchatka but are characterized by remarkably lower enrichment in many lithophile elements than those of the alkaline basalts from this area. The distribution patterns of the basanites display a systematic decrease of normalized concentrations from the group of elements characterized by affinity with melts to the group of compatible elements. This is associated with a deficit in Pb[2] and a weakly pronounced Sr anomaly, which is typical of basanites in both areas. In contrast to the basanites, the alkaline basaltoid of eastern Kamchatka show deep minima not only at Pb but also at K and Rb. The Miocene basanites of eastern and western Kamchatka

[2] For normalized rock compositions, the Pb concentration in the primitive mantle is assumed equal to 0.15 ppm (Sun and McDonough, 1989).

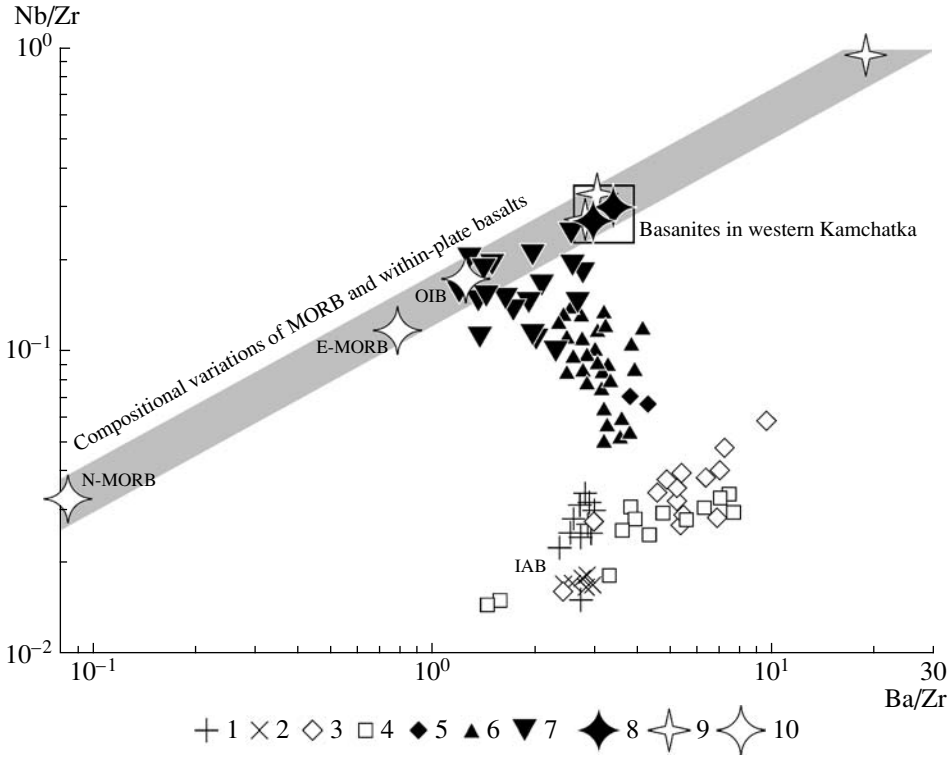

Fig. 6. Nb/Zr–Ba/Zr diagram for the Mount Khukhch basanites and basaltoids of various geodynamic types elsewhere in Kamchatka.

Island-arc basaltoids (IAB): (1) moderate-K basalts of the volcanic belt in eastern Kamchatka; (2) same, for Klyuchevskoi volcano, Central Kamchatkan Depression; (3) moderate- and high-K basaltoids of the volcanic belt in the Sredinyi Range of Kamchatka; (4) basaltoids of the potassic alkaline and subalkaline series in western Kamchatka (absarokites, trachybasalts, and shonkinites); (5) K–Na shonkinites in western Kamchatka; (6) basalts of the K–Na alkaline basaltic and alkaline olivine basaltic series in the Sredinnyi range; (7) basaltoids of the K–Na alkaline and subalkaline series in eastern Kamchatka; (8) basanites at Mount Khukhch, western Kamchatka; (9) average compositions of basanites and alkaline basalts of the African Rift System, Rungwe province, Tanzania (Ivanov et al., 1998), Chad (Gourgaud and Vincent, 2004), Oman (Worthing and Wilde, 2002); (10) compositions of mid-oceanic ridge basalts of normal (N-MORB) and enriched (E-MORB) types and oceanic-island basalts (OIB) (Sun and McDonough, 1989).

Here and below, all geochemical types of basalts from Kamchatka are characterized by our original ICP-MS analytical data and literature materials from (*1*) (Grib et al., 2003), (*2*) (Churikova et al., 2001), (*4*, *5*) (Perepelov et al., 2001), (*6*) (Churikova et al., 2001; Ivanov et al., 2004), (*7*) (Volynets et al., 1990a, 1997; Tikhomirova, 1994).

display significant compositional similarities with the basalts of oceanic islands (OIB) and differ from them only in having somewhat lower concentrations of Zr, Hf, and some REE. It should be mentioned that Zr and Hf minima in the plots are characteristic of basanites and alkaline basalts of many continental rifts (Fig. 7), and some researchers (Gourgaud and Vincent, 2004; Worthing and Wilde, 2002) believe that these minima reflect the conditions of magma generation and the composition of the source.

The $^{87}Sr/^{86}Sr$ isotopic ratio of the Mount Khukhch basanites is equal to 0.70299 ± 0.00010 for sample PP-2264 and 0.70298 ± 0.00015 (2σ) for sample PP-2265. These values correspond to the mantle isotopic signatures within the ranges typical of MORB-type basaltoids.

CRYSTALLIZATION CONDITIONS

Our model simulations of the conditions under which the basanites crystallized were based on the data of petrographic observations and microanalytical examination of mineral assemblages.

The crystallization of significant volumes of olivine phenocrysts and subphenocrysts during early stages (up to 20 vol %) and clinopyroxene and plagioclase subphenocrysts and microlites during the late crystallization stages of the melt (up to 25%) determined the systematic variations in the composition of the residual melt. The systematic evolution of the mineral assemblages with discrete distributions of the compositions and sizes of crystalline phases, as well as the observed resorption and melting of olivine phenocrysts, testify to significant variations in the *P–T* conditions during the crystallization of the melt.

The evolution of the basanite melt can be subdivided into the following stages: (1) crystallization in a deep-seated reservoir (high-pressure stable conditions), (2) deceleration or even termination of crystallization during rapid magma ascent to upper lithospheric levels

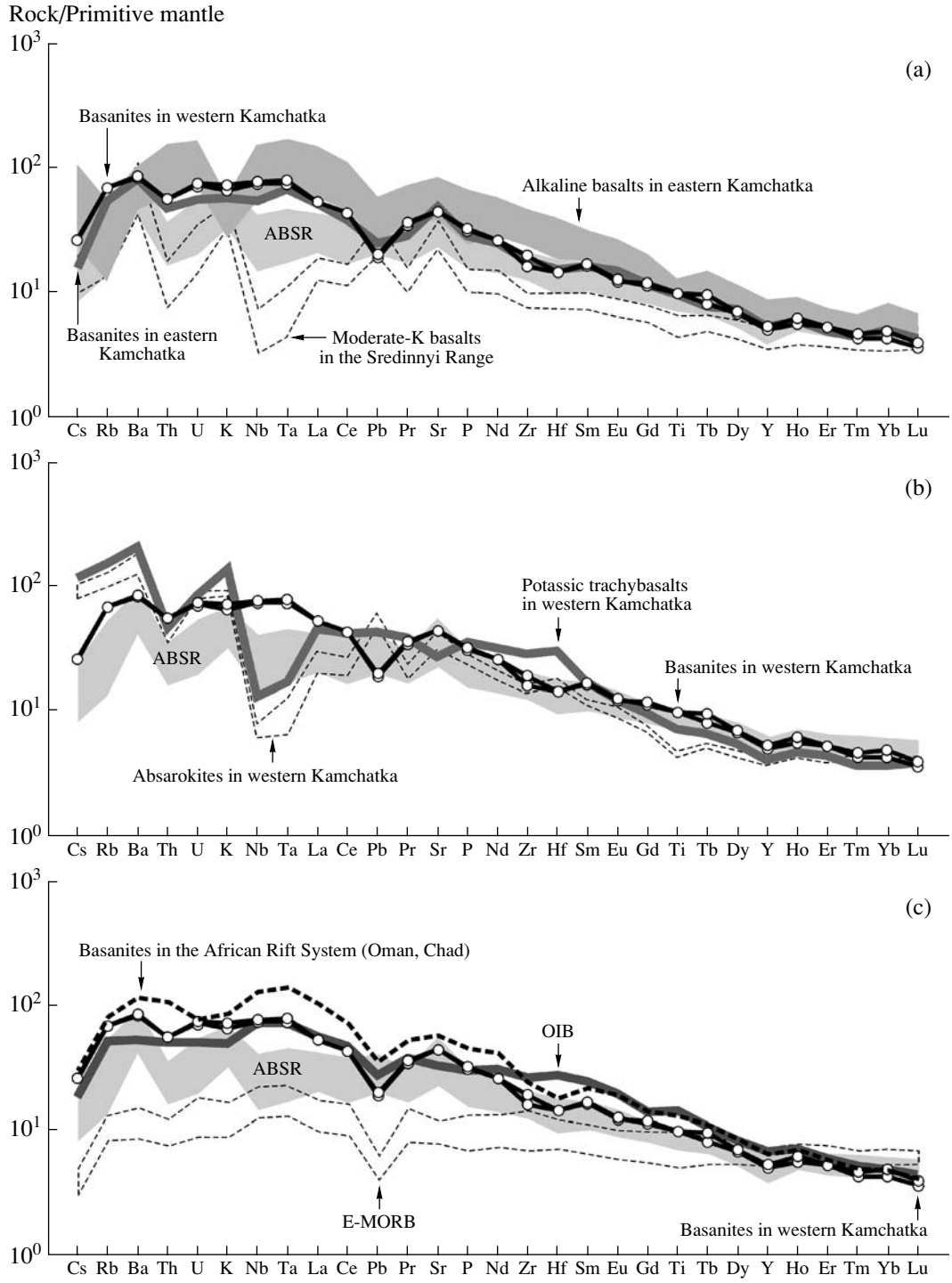

Fig. 7. Distributions of magmophile elements in the Mount Khukhch basanites and basaltoids from various geodynamic environments elsewhere in Kamchatka.

Concentrations of elements (ppm) in the rocks are normalized to their concentrations in "pyrolite" (primitive mantle) (Sun and McDonough, 1989). *ABSR*—nepheline-normative basalts of the alkaline basaltic and alkaline olivine basaltic series in the Sredinnyi Range, Kamchatka. In Fig. 7c, the lower boundary for the E-MORB field corresponds to the average composition of E-MORB (Sun and McDonough, 1989), and the upper boundary of the E-MORB field is drawn according to the average composition of glasses from E-MORB basalts (data of GERM Project, 37 samples); the plot for basanites from the African Rift System is based on the average values of five samples (Gourgaud and Vincent, 2004; Worthing and Wilde, 2002).

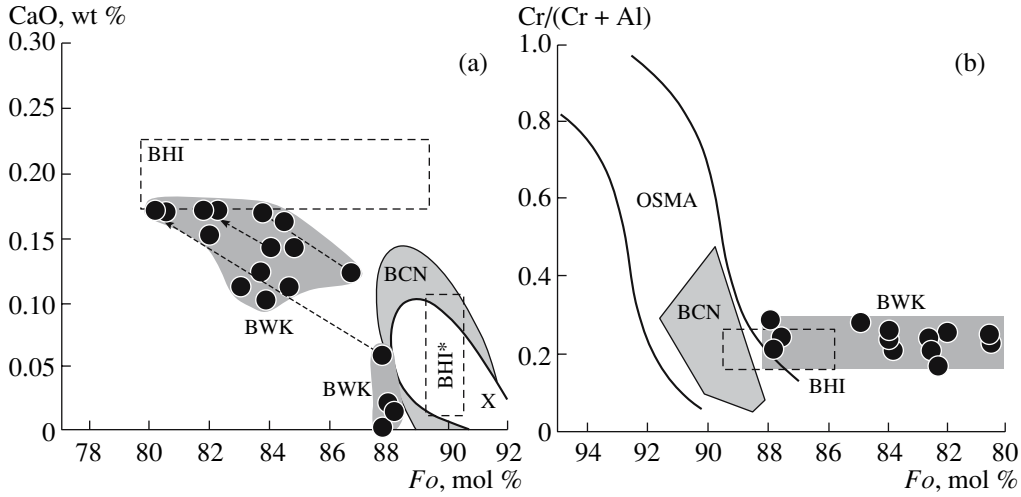

Fig. 8. Correlation between the compositions of (a) olivine phenocrysts and (b) the olivine–spinel assemblage in basanites from western Kamchatka, Hawaii, and mantle mineral associations.

BHI—olivine and olivine–spinel assemblages in basanites from Hawaii, BHI*—same, supposedly xenogenic (Sobolev and Nikogosyan, 1994), BWK—olivine and olivine–spinel assemblages in basanites from western Kamchatka; X—olivine in mantle xenoliths (Hervig et al., 1986); OSMA—olivine–spinel assemblages in mantle rocks (Arai, 1992); BCN—olivine and olivine–spinel assemblages in xenogenic websterite and lherzolite nodules from basanites in cape Navarin, Chukot Peninsula (Koloskov, 1999). Dashed lines with arrowheads connect compositional data points for zonal olivine crystals.

(high-gradient *P–T* conditions), and (3) in-situ crystallization of the magmatic melt in a subvolcanic reservoir (low-pressure conditions). The overall tendency toward a pressure and temperature decrease can be inferred from the analysis of the composition of successively crystallizing mineral phases. For example, the transition from the cores of olivine phenocrysts and rare clinopyroxene phenocrysts to their intermediate zones and subphenocrysts is marked with a systematic increase in the fe# of minerals (Tables 1, 2), which suggests a decrease in the crystallization temperature, and the significant increase in the CaO concentrations in zonal olivine phenocrysts (Fig. 8) provides evidence of a pressure decrease.

In order to test these ideas, we evaluated the *P–T* conditions under which the basanite melt crystallized on the basis of experimental geothermometers (Kodo and Weill, 1970; Peterson, 1989; Putirka, 1997, 2005a, 2005b) and a geothermobarometer (Putirka et al., 2003). The principal criteria applied in selecting from among geothermometers were the correspondence of the composition of our basanites to the compositional range of the experimental silicate materials and the minimum deviation of the calculated temperatures from those measured in the experiments. The choice of the geothermometers (which are based on mineral–melt system for olivine, clinopyroxene, plagioclase, and nepheline) allowed us to obtain consistent ranges of the crystallization temperatures for the basanite melt with a standard error of no more than 30–50°C.

Because of the absence of data on melt inclusions in olivine of the early stage of basanite crystallization, it is not possible to accurately enough assay the composition of the parental basanite melt. The comparison of the *Ol–Spl* association in the basanites and in mantle rocks indicates (Fig. 8) that the most magnesian and lowest-Ca olivine ($Fo_{88.1–87.8}$) in the basanites have CaO concentrations close to those in mantle olivine, and spinel in these associations have similar Cr/(Cr + Al) ratios. Olivine from the basanites differs from that mineral in mantle rocks in having a higher fe#, whereas spinel from the former rocks is richer in TiO_2 (0.95–2.66 wt %) compared with its mantle analogue. These chemical features of the early olivine population and, correspondingly, spinel inclusions in this olivine make it difficult to ascribe them to xenogenic mantle phases. At the same time, this mineral assemblage can be considered within the framework of the model of equilibrium crystallization of the parental basanite melt.

The parental melt assumed in our simulations corresponded to the average bulk composition of the basanites (Table 5, Lq_1). The testing of its equilibrium with the most magnesian cores of olivine phenocrysts of the composition $Fo_{88.1–87.8}$ yielded positive results ($KD_{Fe^{2+}/Mg} = 0.29–0.32$).[3]

In order to determine the crystallization temperatures of mineral assemblages of the basanites according to their inferred crystal sequence, we calculated a succession of the model compositions of the melts (Table 5). Melt composition Lq_4 (Table 5) whose

[3] The Fe^{2+}/Fe^{3+} ratio of the melts was calculated for the NNO–WM ($\log f_{O_2}$–*T*°C) buffer equilibrium by the procedure from (Putirka, 2005a).

Table 5. Comparison of the compositions (wt %) and crystallization temperatures of experimental (Sack et al., 1987) and model basanite melts under atmospheric pressure

Component	1	2	3	4	5	6	7	8	9
	6-S	Lq_1	6-(39)	Lq_2	6-(40)	Lq_3	6-(43)	Lq_4	Lq_5
SiO_2	44.28	43.66	44.29	44.07	44.49	44.47	45.42	45.28	48.44
TiO_2	2.49	1.96	2.69	2.09	2.90	2.22	3.35	2.47	1.60
Al_2O_3	16.04	14.47	16.93	15.40	17.10	16.33	17.63	18.20	21.96
FeO*	9.85	11.33	10.20	10.84	10.17	10.35	10.71	9.37	5.41
MnO	0.16	0.18	0.16	0.17	0.17	0.17	0.19	0.16	0.11
MgO	9.74	10.98	7.94	9.13	6.60	7.29	3.52	3.60	3.34
CaO	12.49	9.82	12.58	10.45	12.81	11.09	8.79	12.35	10.07
Na_2O	3.07	3.43	3.20	3.66	3.23	3.88	5.30	4.34	6.61
K_2O	1.46	2.01	1.56	2.14	2.01	2.27	3.70	2.54	2.46
P_2O_5	0.42	0.66	0.45	0.70	0.53	0.75	1.38	0.83	
H_2O*		0.68		0.72		0.75		0.88	
Total	100.00	99.27	100.00	99.43	100.00	99.62	100.00	100.01	100.00
Fo		88–87	85.5	85–84	83.5	83–82	71.4	73–67	
T_{meas}, °C			1234		1201		1121		
T_{calc}, °C		1227–1226	1194	1210–1207	1175	1184–1182	1129	1123–1119	
f	49.9	51.2	55.7	54.6	60.0	59.1	74.3	72.6	62.3

Note: (**1**, **3**, **5**, and **7**) Initial composition (6-S) and the composition of quenched glasses from the experiments (Sack et al., 1987), according to the INFOREX database (Ariskin et al., 1997) (analysis numbers are retained). (**2**, **4**, **6**, **8**, and **9**) Compositions of model melts used to calculate the crystallization temperatures of basanites from western Kamchatka (see text). All Fe is recalculated to FeO*. Composition Lq_5 was normalized to 100%. T_{meas}, °C is the temperature measured in experiments, T_{calc}, °C is the temperature calculated for olivine crystallization by the olivine–melt geothermometer (Putirka, 1997). H_2O* is the observed and calculated water contents without corrections for water contents in the initial melt (2%, see text). *Fo* is the concentration of the forsterite end member in olivine, f = (FeO* + MnO)/(FeO* + MnO + MgO) is the Fe mole fractions of melts.

$KD_{Fe^{2+}/Mg}$ value corresponded to the equilibrium crystallization of clinopyroxene subphenocrysts and microlites from it (mg# = 71–68), together with subphenocrysts and microlites of plagioclase and titanomagnetite was calculated as residual. It was formed by the crystallization of olivine in association with spinel from the initial basanite melt, whose composition was thus calculated from the composition of initial melt Lq_1 by subtracting the volumes of phases counted in the rocks: 20 vol % olivine and 0.2 vol % spinel. The compositions of the subtracted phases were calculated as averages of 21 analyses of olivine and nine analyses of spinel.

In order to calculate the equilibrium crystallization temperatures of the whole crystallization sequence of olivine phenocrysts and subphenocrysts, we determined intermediate model compositions Lq_2 and Lq_3 (Table 5). The former was calculated as an average of the initial (Lq_1) and residual (Lq_4) basanite melts, and the composition of melt Lq_3 was taken up as the average of intermediate melt Lq_2 and residual melt Lq_4. Melt Lq_2 was determined to have $KD_{Fe^{2+}/Mg}$ = 0.30–0.32 corresponding to the equilibrium crystallization of the cores and intermediate zones of olivine phenocrysts ($Fo_{85–84}$) from this melt. Melt Lq_3 corresponds to the conditions of the equilibrium crystallization of such mineral phases as the marginal zones of olivine phenocrysts and the cores of its microlites $Fo_{83–79}$ ($KD_{Fe^{2+}/Mg}$ = 0.31–0.33) and the cores and intermediate zones of rare clinopyroxene phenocrysts (mg# = 80–75). Residual melt Lq_5 composition (Table 5) for the final crystallization stages of the basanite magma was determined from the results of microprobe rastering and corresponded to the average composition of the basanite groundmass. The choice of these model compositions allowed us to obtain all principal mineral assemblages (*Ol* + *Spl*, *Ol* + *Cpx*, *Cpx* + *Pl*, and *Pl* + *Ne*) in our simulations of the equilibrium crystallization of basanites. The accuracy of our model simulations is confirmed by the compatibility of their results and the quench glasses successively obtained in the experiments (Sack et al., 1987) with the starting composition close to that of our basanites (Table 5).

The *P–T* conditions determined for the crystallization of the basanite melt are listed in Table 6. All calculations of experimental geothermometers display sys-

Table 6. Crystallization temperatures and pressures calculated for basanites from western Kamchatka

Geothermometer		*P*, kbar	*Ol*–Lq (±42)	*Cpx*–Lq (±34)	*Pl*–Lq (±37)	*Pl*–Lq (±34)	*Ne*–Lq (±30)
1		2	3	4	5	6	7
I	$Ol_{Fo\ 88–86} + Spl_{\text{mg\# }56–52} + Lq_1$		1372–1369 (4)				
II	$Ol_{Fo\ 85–84} + Spl_{\text{mg\# }49–47} + Lq_2$		1311–1298 (9)				
III	$Ol_{Fo\ 83–79} + Cpx_{\text{mg\# }80–75} + Lq_3$	9–10 (±1.7)	1226–1210 (6)	1194–1184 (5)			
IV	$Cpx_{\text{mg\# }73–68} + Pl_{An\ 74–67} + \text{Ti-}Mag + Lq_4$	1.5–3 (±1.7)		1115–1097 (7)	1138–1133 (8)	1149–1111 (8)	
V	$Cpx_{\text{mg\# }77–74} + Pl_{An\ 67–57} + \text{Ti-}Mag + Lq_5$	0.5–1 (±1.7)		1058–1048 (7)	1060–1053 (10)	1121–1075 (10)	
VI	$Pl_{An\ 50–21} + Ne + Lq_5$	<0.5			1001–889 (6)	1051–883 (6)	1014–935 (12)

Note: (**1**) Compositions of mineral assemblages: (**I**–**III**) assemblages of the early populations of olivine phenocrysts, spinel inclusions in them, and clinopyroxene phenocrysts; (**IV**, **V**) assemblages of the early populations of subphenocrysts and microlites (massive crystallization), (**VI**) assemblage of the microlites and interstitial phases of the final crystallization stage of the melt. (**2**) Average estimates and standard errors (in parentheses) of the crystallization pressure determined by the clinopyroxene geobarometer (Putirka et al., 2003, model A). Calculated crystallization temperatures of mineral assemblages (*T*, °C): (**3**) by the olivine–melt geothermometer (Putirka, 2005a, model C), with corrections for water concentrations in the melt; (**4**) by the clinopyroxene–melt geothermometer (Putirka et al., 2003, model B); (**5**) by the plagioclase–melt geothermometer (Putirka, 2005b, models A and H); (**6**) by the plagioclase–melt geothermometer at P_{H_2O} = 1.0 kbar (Kudo and Weill, 1970); (**7**) by the nepheline–melt geothermometer (Peterson, 1989);

Fo and *An* are the concentrations of the forsterite and anorthite end members in olivine and plagioclase; mg# = Mg/(Mg + Fe + Mn), at %—Mg mole fraction of spinel and clinopyroxene. Numerals in the first line are the standard errors of temperatures determined by the geothermometers; columns **3** through **7** list the number of mineral–melt pairs used to calculate the equilibrium crystallization temperatures. See text for other details.

tematic evolution from high-temperature to relatively low-temperature mineral assemblages.

The crystallization temperatures of the first liquidus phases of olivine $Fo_{88–87}$ from parental basanite melt Lq_1 were assayed at 1372–1369°C (Table 6). The substitution of these temperatures of the melt into the Albarede (1992) empirical formula indicates that the conditions of mantle equilibrium could be reached by the melt under pressures of 25–26 kbar. These are the highest values for this magmatic system, but they are likely lower than the conditions under which the parental melt was formed. The pressures of discrete crystallization stages of the basanite melt with the formation of mineral assemblages with clinopyroxene (model compositions Lq_3 and Lq_4) were evaluated by the geobarometer (Putirka et al., 2003; model A). The calculation results demonstrate a pressure decrease during the evolution of the magmatic system (Table 6).

In compliance with the correlations previously established for the compositions of the initial alkaline magmas (H_2O/P_2O_5 = 3; Dixon et al., 1997) and tholeiitic magmas ($H_2O/K_2O \approx 1$; Hauri, 2002), we assumed that the crystallization of the high-temperature mineral assemblages took place in the basanite melt with H_2O concentrations close to 2.0 wt %. This value corresponds to the values of the aforementioned ratios for the parental basanite melt: H_2O/K_2O = 2.11–1.90 and H_2O/P_2O_5 = 2.01–1.95 (Table 4). The crystallization temperatures calculated for the assemblages of subphenocrysts and microlites of *Pl* + *Cpx* in equilibrium with model residual melt Lq_4 are consistent only if the H_2O concentration in the magmatic system is further increased. Under a total pressure of 1.5–3 kbar, the crystallization temperatures of plagioclase and clinopyroxene in melt Lq_4 are comparable if corrections are introduced for a water content in the melt equal 2.5 wt %, and the water concentration during plagioclase $An_{66–57}$ crystallization from residual melt Lq_5 corresponding to the composition of the basanite groundmass was estimated at 3.9–5.1 wt % (Putirka, 2005b, models A and H; Ariskin and Barmina, 2000) (Table 6). The calculation of the compositions of model melts Lq_2, Lq_3, and Lq_4 based on the estimation of the H_2O concentration in the parental basanite melt suggests an increase in the water concentrations in these melts to 2.14, 2.27, and 2.54 wt %, respectively. These values were used to calculate the crystallization temperatures of olivine and clinopyroxene from the basanite melt (Table 6). It should be mentioned that the assumed H_2O content in the initial basanite melt (2 wt %) corresponds to the calculated value for the parental nephelinites magmas of Hawaii (2 wt %; Dixon et al., 1997).

Calculations by the method (Almeev and Ariskin, 1996) at $P_{tot} = P_{H_2O}$ = 1.5 kbar and temperatures of

1080–1140°C indicate that the water solubility in residual basanite melt Lq_4 is ~4.9–5.5 wt %, and that in melt Lq_5 at $P_{tot} = P_{H_2O} = 1$ kbar and temperatures of 890–1120°C is 5.9 wt %. The temperatures calculated by the plagioclase–melt geothermometers (Putirka, 2005b, Kudo and Weill, 1970) for the final crystallization stages of the basanite melt are consistent at a water pressure of ~1 kbar. It is thus reasonable to believe that, under a generally elevated water pressure during the crystallization of the basanite melt, only the crystallization of microlites and interstitial phases could take place under conditions approaching saturation with respect to water. This finds support in, for example, the occurrence of interstitial analcime in the rocks.

At the same time, it is hard to estimate the concentrations of volatiles during the crystallization of the melt in the subvolcanic reservoir, because the evolution of the basanite magma during this stage proceeded under a low lithostatic pressure, a high permeability of the system, and was associated with magma degassing, as is typical of these conditions. For example, the H_2O and CO_2 concentrations in the basanites without traces of secondary alterations were 0.55–0.80 and 0.17–0.23 wt %, respectively (Table 6). The observed CO_2 concentrations correspond to the limit for the CO_2 solubility in basanite melts under pressures of 2–2.5 kbar (Lowenstern, 2001), while the dependences $CO_2 = (2.5 \pm 1.5)H_2O$ established for the initial alkaline basaltoid magmas (Dixon et al., 1997) suggest much higher initial CO_2 concentrations of 2–8 wt %. Proceeding from the aforementioned estimates, the losses of volatiles during the evolution of the basanite magma could be 60–72 wt % for H_2O and 92–97 wt % for CO_2.

The comparison of the results of our model simulations and data on the compositional evolution of olivine and clinopyroxene phenocrysts suggests that the latter should have crystallized from a basanite melt at a systematic temperature decrease (Table 6). The crystallization temperatures of the first liquidus phases, the most magnesian olivine and spinel, from the parental basanite melt were estimated at ~1372–1369°C. During the subsequent crystallization of the olivine–spinel assemblage, the temperature decreased to 1311–1298°C. This stage ended with the formation of clinopyroxene phenocrysts at temperatures of 1226–1184°C and pressures of approximately 9–10 kbar. The further drastic decrease in pressure and, to a lesser degree, temperature were likely associated with the deceleration or even termination of the crystallization of the basanite melt in the magmatic system. The massive crystallization of the *Cpx + Pl + TiMag* subphenocrysts and microlites occurred at lower temperatures of ~1149–1048°C and much lower estimated pressures of ~0.5–3 kbar. These crystallization conditions corresponded to the stage when the subvolcanic reservoir was formed as a result of magma ascent to the surface. The crystallization process of the basanite melt ended in a shallow magmatic chamber with the origin of the assemblage of microlites of the most sodic plagioclase $An_{50–21}$ and apatite, along with interstitial nepheline, leucite, and analcime as the temperature decreased to ~935–883°C.

The temperature estimates presented above for the crystallization of basanite melts in western Kamchatka are close to the estimated crystallization conditions of the olivine + clinopyroxene assemblage in the initial basanite magmas of the Hawaiian Islands: 1390–1170°C (Sobolev and Nikogosyan, 1994).

The high crystallization temperatures of the first liquidus mineral phases (*Ol + Spl*), the pressures of the mantle equilibrium of the initial melt, and the trace-element characteristics of the rocks are generally consistent with the model of the derivation of basanite magma under the conditions of the garnet depth facies in the mantle. The range of the La_N/Yb_N and Dy_N/Yb_N ratios in the rocks, and the Yb_N concentration normalized to chondrite (10.8–12.6, 1.4–1.6, and 11.5–13.3, respectively) correspond to the model of ~6% partial melting of garnet-bearing peridotite (Ivanov et al., 1998). With regard for the standard errors of the geothermometers, the model crystallization temperatures of the *Ol + Spl* assemblage in equilibrium with the initial basanite melt exceed not only the value of 1300°C (the potential temperature of the normal mantle) but even 1333°C (the temperature in the bottom of the boundary thermal layer) (McKenzie and Bickle, 1988; Harry and Leeman, 1995). This led us to hypothesize that the appearance of the Neogene alkaline basite magmas in the backarc geodynamic environment of western Kamchatka was associated with magma generation at the relative heating of the mantle and the corresponding thinning of the lithosphere, as is typical of active rifting.

GEODYNAMIC SETTING OF BASANITES IN WESTERN KAMCHATKA

Judging from the setting of the Mount Khukhch basanite body in the structure of the sedimentary cover of western Kamchatka and according to the dating of related trachybasalt stocks and dikes (8–17 Ma, K–Ar; Koval' and Adamchuk, 1986), the age of the body is close to the age range of alkaline basaltic magmatism in eastern Kamchatka (5–14 Ma, Volynets et al., 1997, 1990a), i.e., Middle–Late Miocene. However, the later instrumental dating of the basanites themselves does not rule out the possibility of refining their age within the Middle Miocene–Early Pliocene range. Taking into account the position of the backarc territory of western Kamchatka relative to the front of modern Pliocene–Quaternary subduction zone, the development of magmatic processes of the within-plate type could be much more protracted, in contrast to eastern Kamchatka (Volynets et al., 1990a). Similarities between the compositions and ages of the basaltoid rocks of the within-plate geochemical type in eastern and western Kamchatka testify to the nearly coeval derivation of K–Na alkaline magmas beneath areas separated by a territory

about 300 km wide across the strike of the major island-arc structure. The geodynamic setting of alkaline basaltic magmatism in western and eastern Kamchatka was controlled mostly by the termination of the Oligocene–Early Miocene subduction of the Kula oceanic plate beneath the continental margin of Kamchatka and the development of rifting up to the onset of a new episode of Pliocene–Quaternary subduction of the Pacific oceanic plate. The age of alkaline basaltic magmatism in Kamchatka is consistent with the timing of the most intense extension in marginal seas in the West Pacific, which were marked first by northward strike-slip faulting and then by rifting and spreading structures (Filatova and Fedorov, 2003). At this time, during the transformation of the convergent margin of the Asian continental and oceanic plates into a transform margin, deep faulting of the lithosphere and decompressional magma generation coupled with the relative heating of the mantle could be favorable for the origin of basite magmas both at the front of the consolidated continental block of Kamchatka and in its rear portions. The geodynamic setting of basanites in western Kamchatka is generally consistent with the earlier conclusions (Volynets et al., 1990a, 1997) about the position of Neogene alkaline magmatism in eastern Kamchatka.

CONCLUSIONS

The results obtained in the course of the mineralogical–geochemical studying of nepheline- and leucite-bearing basanites from Mount Khukhch in western Kamchatka and the revision of preexisting data demonstrate that the find of these rocks is the first reliable piece of evidence of the occurrence of typical within-plate magmas in the rear zone of the Kamchatkan arc system. Conceivably, the area of K–Na alkaline Late Paleogene–Neogene magmatism in this territory can be extended based on the results of further research and the discovery of a broad spectrum of the compositions of magmatic rocks typical of rifting environments, such as OIB and E-MORB. Rocks of such composition seem to be found in the basin of the Bystraya River: these are Late Paleogene–Neogene essexite-diabase dikes (Koval' and Adamchuk, 1986). This idea is underlain by the presence of at least two long time intervals in the Cenozoic evolutionary history of the Pacific sector of the Kamchatkan arc system: Late Eocene–Early Oligocene and Middle–Late Miocene, which were marked by the absence of active subduction and, perhaps, by the development of not only collisional but also rifting processes (Bogdanov ad Chekhovich, 2002, 2004). The duration of each of these intervals was close to 10 Ma, i.e., was long enough for a change in the geodynamic regimes and environments of magma generation in the development of large geologic structures near active convergent plate boundaries.

ACKNOWLEDGMENTS

The field study of magmatic rocks in western Kamchatka in 2001 was made possible by A.A. Glukh, the head of the Khairyuzovskaya Geological Survey Team of the Kamchatgeologiya Sate Enterprise, and P.F. Petrochenko, a geologist of the team, M.A. Talalai, the head of the Central Geochemical Team of the Kamchatskaya Survey Expedition, and V.V. Khlopkov, a geologist of the expedition, as well as Dr. M.M. Pevzner of the Geological Institute (GIN), Russian Academy of Sciences. The critical analysis of the manuscript conducted by the Corresponding Member of the Russian Academy of Sciences A.I. Khanchuk and Dr. Yu.A. Martynov of the Far East Geological Institute, Far East Division, Russian Academy of Sciences, helped the authors to improve its content. The authors thank all of the aforementioned persons. Special thanks are due to the Corresponding Member of the Russian Academy of Sciences A.V. Sobolev, whose analysis of the manuscript led the authors to profoundly re-conceptualize their data and refine certain petrological conclusions arrived at solving problems related to the genesis and crystallization of basite magmas. The study was financially supported by the Russian Foundation for Basic Research (project no. 04-05-64800) and the Program for Support of Leading Research Schools (grant nos. NSH-2294.2003.5 and NSH-5439.2006.9) and Integration Project 6.9 of the Siberian Division, Russian Academy of Sciences.

REFERENCES

1. R. R. Al'meev and A. A. Ariskin, "Mineral–Melt Equilibria in a Hydrous Basaltic System: Computer Modeling," Geokhimiya, No. 7, 624–636 (1996) [Geochem. Int. **34**, 563–573 (1996)].
2. F. Albarede, "How Deep do Common Basaltic Magmas from and Differentiate," J. Geophys. Res. **97** (B7), 10997–11009 (1992).
3. M. P. Antipov, Yu. B. Gladenkov, A. V. Zhuravlev, and A. E. Shchantser, "Structure of the near-Kamchatka Area of the Sea of Okhotsk Floor and its Cenozoic History," Byull. Mosk. O–va Ispyt. Prir., Otd. Geol. **72** (2), 19–25 (1997).
4. S. Arai, "Chemistry of Chromian Spinel in Volcanic Rocks as a Potential Guide to Magma Chemistry," Mineral. Mag. **56**, 173–184 (1992).
5. A. A. Ariskin and G. S. Barmina, *Simulation of Phase Equilibria during Crystallization of the Basaltic Magmas* (Nauka, Moscow, 2000) [in Russian].
6. A. A. Ariskin, S. S. Meshalkin, R. R. Al'meev, et al., "INFOREX Information Retrieval System: Analysis and Processing of Experimental Data on Phase Equilibria in Igneous Rocks," Petrologiya **5**, 42–67 (1997) [Petrology **5**, 28–36 (1997)].
7. N. A. Bogdanov and V. D. Chekhovich, "Geodynamic Aspects of Cenozoic Continental Margin Volcanism of the Pacific and Bering Sea Sectors of Kamchatka," Geol. Geofiz. **45** (4), 421–429 (2004).
8. N. A. Bogdanov and V. D. Chekhovich, "On the Collision between the West Kamchatka and Sea of Okhotsk

Plates," Geotektonika, No. 1, 72–85 (2002) [Geotectonics **36**, 63–75 (2002)].

9. T. Churikova, F. Dorendorf, and G. Worner, "Sources and Fluids in the Mantle Wedge below Kamchatka, Evidence from Across-Arc Geochemical Variation," J. Petrol. **42**, 1567–1593 (2001).
10. W. A. Deer, R. A. Howie, and J. Zussman, *Rock-Forming Minerals. Vol. 4. Framework Silicates* (Longman, London, 1962; Mir, Moscow, 1966) [in Russian].
11. E. Dixon, D. A. Clague, P. Wallace, and P. Poreda, "Volatiles in Alkalic Basalts from the North Arch Volcanic Field, Hawaii: Extensive Degassing of Deep Submarine-Erupted Alkalic Series Lavas," J. Petrol. **38**, 911–939 (1997).
12. F. Dorendorf, T. Churikova, A. Koloskov, and G. Worner, "Late Pleistocene to Holocene Activity at Bakening Volcano and Surrounding Monogenetic Centers (Kamchatka): Volcanic Geology and Geochemical Evolution," J. Volcanol. Geotherm. Res. **104**, 131–151 (2000).
13. N. I. Filatova and P. I. Fedorov, "Cenozoic Magmatism in the Korean-Japanese Region and Its Geodynamic Setting," Geotektonika, No. 1, 54–77 (2003) [Geotectonics **37**, 49–70 (2003)].
14. G. B. Flerov, A. V. Koloskov, and S. V. Moskaleva, "Leucite and Analcime in the Upper Cretaceous–Paleogene Potassium Basaltoids, Central Kamchatka," Dokl. Akad. Nauk **362** (1), 87–89 (1998) [Dokl. Earth Sci. **362**, 912–914 (1998)].
15. *Geological and Mineral Resources Maps for Kamchatka District and Koryak Autonomous Okrug. Scale 1 : 1500000*, Ed. by A. F. Litvinov, B. A. Markovskii, and V. P. Zaitsev (VSEGEI, St. Petersburg, 2005) [in Russian].
16. Yu. B. Gladenkov, B. A. Sal'nikov, A. K. Borovtsev, et al., *Solution of the Working Interdisciplinary Regional Stratigraphic Conferences on Paleogene and Neogene of the Eastern Russia—Kamchatka, Koryak Highland, Sakhalin and Kurile Islands. Explanatory Note to Stratigraphic Schemes* (GEOS, Moscow, 1998) [in Russian].
17. A. Gourgaud and P. M. Vincent, "Petrology of Two Continental Alkaline Intraplate Series at Emi Koussi Volcano, Tibesti, Chad," J. Volcanol. Geotherm. Res. **129**, 261–290 (2004).
18. D.H. Green, T. J. Faloon, S. M. Eggins, and G. M. Yaxley, "Primary Magmas and Mantle Temperatures," Eur. J. Mineral. **13**, 437–451 (2001).
19. E. N. Grib, A. B. Perepelov, and V. L. Leonov, "Geochemistry of the Volcanic Rocks of the Uzon–Geizer Depression," Vulkanol. Seismol., No. 4, 11–28 (2003).
20. I. S. Guziev, "Alkaline Olivine–Basalt Association of Western Kamchatka," in *Volcanism and Geochemistry of Its Products* (Nauka, Moscow, 1967), pp. 126–144 [in Russian].
21. D. Harry and W. P. Leeman, "Partial Melting of Metasomatized Subcontinental Mantle and the Magma Source Potential of the Lower Lithosphere," J. Geophys. Res. **100**, 10255–10269 (1995).
22. E. Hauri, "SIMS Analysis of Volatiles in Silicate Glasses, 2: Isotopes and Abundances in Hawaiian Melt Inclusions," Chem. Geology **183**, 115–141 (2002).
23. R. Hervig, J. V. Smith, and J. B. Dawson, "Lherzolite Xenoliths in Kimberlites and Basalts: Petrogenetic and Crystallochemical Significance of Some Minor and Trace Elements in Olivine, Pyroxene, Garnet and Spinel," Earth Sci. **77**, 181–201 (1986).
24. A. V. Ivanov, A. B. Perepelov, M. Yu. Puzankov, et al., "Rift- and Arc-Type Basaltic Volcanism of the Sredinny Ridge, Kamchatka: Case Study of the Payalpan Volcano-Tectonic Structure," in *Metallogeny of the Pacific Northwest: Tectonics, Magmatism and Metallogeny of Active Continental Margins* (Dalnauka, Vladivostok, 2004), pp. 345–349 [in Russian].
25. A. V. Ivanov, S. V. Rasskazov, E. P. Chebykin, et al., "Y/Ho Ratios in the Late Cenozoic Basalts from Eastern Tuva, Russia: an ICP-MS Study with Enhanced Data Quality," Geostand. Newslett. J. Geostand. Geoanal. **24**, 197–204 (2000).
26. A. V. Ivanov, S. V. Rasskazov, A. Boven, et al., "Late Cenozoic Alkaline-Ultrabasic and Alkaline Basanite Magmatism of the Rungwe Province, Tanzania," Petrologiya **6**, 228–250 (1998) [Petrology **6**, 208–229 (1998)].
27. A. V. Koloskov, *Ultramafic Inclusions in the Volcanic Rocks as Self-Regulating Geological System* (Nauchnyi Mir, Moscow, 1999) [in Russian].
28. E. A. Konstantinovskaya, *Tectonics of the East Asian Margin: Structural Evolution and Geodynamic Modeling* (Nauchnyi Mir, Moscow, 2003) [in Russian].
29. P. A. Koval' and G. L. Adamchuk, *Explanatory Note to Geological Map on a Scale 1 : 200000. Sheet O-57-XXXIII. Western Kamchatka Series, No. 4976/1* (FGU "KamTFGI", Petropavlovsk-Kamchatskii, 1986) [in Russian].
30. A. M. Kudo and D. F. Weill, "An Igneous Plagioclase Thermometer," Contrib. Mineral. Petrol. **25**, 52–65 (1970).
31. M. J. LeBas, R. W. Le Maitre, A. Streckeisen, and B. Zanettin, "A Chemical Classification of Volcanic Rocks Based on the Total Alkali-Silica Diagram," J. Petrol. **27**, 745–750 (1986).
32. V. A. Legler, "Cenozoic Evolution of Kamchatka in the Light of Plate Tectonics," in *Tectonics of Lithospheric Plates* (VINITI, Moscow, 1977), pp. 137–169 [in Russian].
33. J. B. Lowenstern, "Carbon Dioxide in Magmas and Implications for Hydrothermal Systems," Mineral. Deposita **36**, 490–502 (2001).
34. D. P. McKenzie and M. J. Bickle, "The volume and composition of melt generated by extension of the lithosphere," J. Petrol. **29**, 625–679 (1988).
35. T. F. Moroz, *Explanatory Note to the Geological Map on a Scale of 1 : 200 000. Sheet O-57-XXVI. Western Kamchatka Series* (Nedra, Moscow, 1971) [in Russian].
36. A. B. Perepelov, O. N. Volynets, G. N. Anoshin, et al., "Western Kamchatka Alkali-Potassic Basaltoid Volcanism: Geological and Geochemical Review," in *Proceedings of International Workshop on Alkaline Magmatism and the Problems of Mantle Source, Irkutsk, Russia, 2001* (Irkutsk, 2001), pp. 52–69.
37. A. B. Perepelov, A. V. Ivanov, U. S. Makintosh, et al., "Potassic Alkali Magmatism of Western Kamchatka—Late Eocene–Early Oligocene Inversion of Geodynamic

Regimes in the Evolution of Island Arc System," in *All-Russian Scientific Conference Devoted to 10th Anniversary of Russian Foundation for Basic Research. Isotope Geochronology in Solution of the Problems of Geodynamic and Ore Genesis* (Ts. Inf. Kul't., St. Petersburg, 2003), pp. 348–354 [in Russian].

38. T. D. Peterson, "Peralkaline Nephelinites. I. Comparative Petrology of Shombole and Oldonyo Lengai, East Africa," Contrib. Mineral. Petrol. **101**, 458–478 (1989).

39. M. Portnyagin, K. Hoernle, G. Avdeiko, et al., "Transition from Arc to Oceanic Magmatism at the Kamchatka–Aleutian Junction," Geology **33**, 25–28 (2005).

40. K. Putirka, "Magma Transport at Hawaii: Inferences Based on Igneous Thermobarometry," Geology **25**, 69–72 (1997).

41. K. Putirka, "Mantle Potential Temperatures at Hawaii, Iceland, and the Mid-Ocean Ridge System, as Inferred from Olivine Phenocrysts: Evidence for Thermally Driven Mantle Plumes," Geochem., Geophys., Geosyst., Electr. J. Earth Sci. **6** (5) (2005a).

42. K. Putirka, "Igneous Thermometers and Barometers based on Plagioclase + Liquid Equilibria: Tests of Some Existing Models and New Calibrations," Am. Mineral. **90**, 336–346 (2005b).

43. K. Putirka, F. J. Ryerson, and H. Mikaelian, "New Igneous Thermobarometers for Mafic and Evolved Lava Compositions, Based on Clinopyroxene + Liquid Equilibria," Am. Mineral. **88**, 1542–1554 (2003).

44. R. O. Sack, D. Walker, I. S. E. Carmichael, "Experimental Petrology of Alkalic Lavas: Constraints on Cotectics of Multiple Saturation in Natural Basic Liquids," Contrib. Mineral. Petrol. **96**, 1–23 (1987).

45. A. E. Shantser and P. I. Fedorov, "Geochemistry of Lower Paleozoic Rocks of Western Kamchatka," Byull. Mosk. O-va Ispyt. Prir., Otd. Geol. **74** (6), 20–28 (1999).

46. J. F. Schairer, "The Alkali Feldspar Join in the system $NaAlSiO_4$–$KAlSiO_4$–SiO_2," J. Geol. **58**, 512–517 (1950); (*Feldspars*, Inostr. Lit., Moscow, 1952).

47. E. V. Smirnova, I. N. Mysovskaya, V. I. Lozhkin, and N. N. Pakhomova, "Estimate of Spectral Noise during the Use of ELEMENT 2 Magnetic Sector ICP–MS Analyzer: Determination of Rare Earth Elements," in *All-Russian Conference on Analytical Chemistry. Russian Analytics* (Moscow, 2004), pp. 157–158 [in Russian].

48. A. V. Sobolev and I. K. Nikogosyan, "Petrology of Magmatism of Long-Lived Mantle Jets: Hawaiian Islands (Pacific Ocean) and Reunion Island (Indian Ocean)," Petrologiya **2**, 131–168 (1994).

49. A. V. Solov'ev, M. T. Brandon, J. I. Garver, et al., "Collision of the Olyutor Island Arc with the Eurasian Continental Margin: Kinematic and Age Aspects," Dokl. Akad. Nauk **360**, 666–668 (1998) [Dokl. Earth Sci. **361**, 632–634 (1998)].

50. S. S. Sun and W. F. McDonough, "Chemical and Isotopic Systematics of Oceanic Basalts: Implication for Mantle Composition and Processes," in *Magmatism in the Ocean Basins*, Geol. Soc. Spec. Publ. **2**, 313–346 (1989).

51. Y. Tatsumi, T. Kogiso, and S. Nohda, "Formation of a Third Volcanic Chain in Kamchatka: Generation of Unusual Subduction-Related Magmas," Contrib. Mineral. Petrol. **120**, 117–128 (1995).

52. S. R. Tikhomirova, "Late Cenozoic Teschenites of Eastern Kamchatka," Dokl. Akad. Nauk **335**, 626–629 (1994).

53. O. N. Volynets, "Geochemical Types, Petrology and Genesis of Late Cenozoic Volcanic Rocks from the Kurile–Kamchatka Island-Arc System," Int. Geol. Rev. **36**, 373–405 (1994).

54. O. N. Volynets and V. A. Anan'ev, "Leucite and Nepheline in the Quaternary Basalts of Kamchatka," Dokl. Akad. Nauk SSSR **275** (4), 955– 958 (1984).

55. O. N. Volynets, Extended Abstract of Doctoral Dissertation in Geology and Mineralogy (Mosk. Gos. Univ., Moscow, 1993).

56. O. N. Volynets, G. N. Anoshin, Yu. M. Puzankov, et al., "Potassic Basaltoids of Western Kamchatka—Occurrence of the Lamproite Series in the Island Arc System," Geol. Geofiz., No. 11, 41–51 (1987).

57. O. N. Volynets, S. F. Karpenko, R. U. Lei, and M. Gorring, "Isotopic Composition of Late Neogene K–Na Alkaline Basalts of Eastern Kamchatka: Indicators of the Heterogeneity of the Mantle Magma Sources," Geokhimiya, No. 10, 1005–1018 (1997) [Geochem. Int. **35**, 884–896 (1997)].

58. O. N. Volynets, V. S. Antipin, A. B. Perepelov, et al., "Rare Earths in Late Cenozoic High-Potassic Volcanic Rocks of Kamchatka," in *Geochemistry of Volcanic Rocks of Different Geodynamic Settings* (Nauka, Novosibirsk, 1986), pp. 149–165 [in Russian].

59. O. N. Volynets, V. S. Antipin, A. B. Perepelov, and G. N. Anoshin, "Geochemistry of Island-Arc Volcanic Series as Applied to Geodynamics (Kamchatka)," Geol. Geofiz., No. 5, 3–13 (1990b).

60. O. N. Volynets, V. S. Antipin, G. N. Anoshin, et al., "First Data on the Geochemistry and Mineralogy of Late Cenozoic Potassic Basaltoids of Western Kamchatka," Dokl. Akad. Nauk SSSR **284** (1), 205–208 (1985).

61. O. N. Volynets, V. S. Uspenskii, G. N. Anoshin, et al., "Evolution of Geodynamic Regime of Magma Formation at Eastern Kamchatka in Late Conozoic based on Geochemical Data," Vulkanol. Seismol., No. 5, 14–27 (1990a).

62. M. A. Worthing and A. R. Wilde, "Basanites Related to Late Eocene Extension from NE Oman," J. Geol. Soc. London **159**, pp. 469–483 (2002).

63. O. V. Yakubovich and V. I. Tarasov, "Synthesis of Monocrystals and Crystal Structure of Hydronepheline," Dokl. Akad. Nauk SSSR **303**, 1382–1386 (1988).

64. T. A. Yasnygina, S. V. Rasskazov, M. E. Markova, et al., "Determination of Trace Elements in the Mafic–Intermediate Volcanic Rocks by ICP-MS using Microwave Acid Decomposition," in *Applied Geochemistry. Vyp. 4. Analytical Studies*, Ed. by E. K. Burenkov and A. A. Kremenetskii (IMGRE, Moscow, 2003), pp. 48–56 [in Russian].